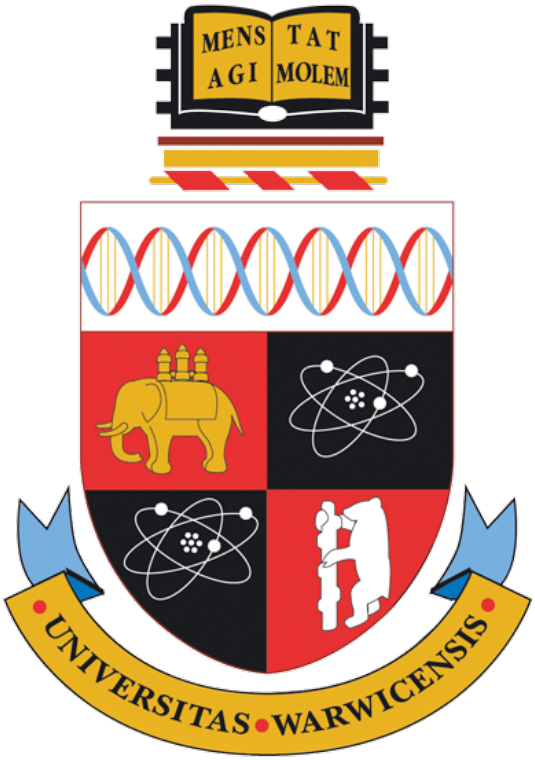

A Study of the Integer Quantum Hall Effect with a Modified Chalker-Coddington Network Model that Incorporates Geometric Disorder

by

Benoit Assi

Thesis

Submitted to the University of Warwick

Master of Science

Department of Physics

April 2019

THE UNIVERSITY OF WARWICK

Contents

List of Tables

List of Figures

Acknowledgments

I would like to begin by thanking R. Romer for supervising this project and imparting some of his immense expertise in condensed matter theory on to me, moreover his patience and support is truly commendable and I appreciate it beyond words can express. I would also like to thank P. Cain for his discussions and insight into the numerical methods employed in the project as well as J. Aarons and E. Carnio for their helpfulness when it came to programming issues, in particular my code could not have been as efficient or MPI compatible without their suggestions. Lastly, I would like to thank my good friend L. Benini, whom with I shared an office and a supervisor and without whom with my life would have been far less enjoyable.

Declarations

I certify that this work contains no material which has been accepted for the award of any other degree or diploma in my name, in any university or other tertiary institution and, to the best of my knowledge and belief, contains no material previously published or written by another person, except where due reference has been made in the text. In addition, I certify that no part of this work will, in the future, be used in a submission in my name, for any other degree or diploma in any university or other tertiary institution without the prior approval of the University of Warwick and where applicable, any partner institution responsible for the joint-award of this degree.

Abstract

This work aims to employ the well known real space renormalisation group method in finding the critical exponent of conductance, ν, of the Chalker-Coddington network model which is postulated to be equivalent to the integer quantum hall exponent. Previous low precision estimates for the critical exponent, ν, have been found to be in the range, $\nu \sim 2.3 - 2.4$ [38, 36, 37, 54, 39, 13], which is close to the recent experimentally observed critical exponent, $\nu_{\text{exp}} \sim 2.38$ [55]. In this thesis, we begin by showing how the critical exponents vary for a range of super unit cell structures in the renormalisation group approach. We find that there exist two types of renormalisation group units that produce the closest values to the integer quantum hall critical exponent as the most recent high accuracy simulation results using the CC network [78, 55, 79, 62, 63, 1, 60] as well as a tight binding model produced [73], $\nu \sim 2.58 - 2.6$. The remainder of the work investigates the recent claim that another type of disorder should also be taken into account - geometric disorder [30]. We present the estimates of critical exponents we found when incorporating various amounts of this disorder, in both the statistically isotropic and anisotropic cases for a range of unit cells. Whence, our findings show that one can tune the critical exponent to a particular value, by adding a set amount of geometric disorder independent of the unit cell employed in the renormalisation group approach.

Chapter 1

Introduction

The integer quantum Hall (IQH) effect, first discovered by Klitzing *et al.* [84], occurs in the study of electrons in a 2D plane with a magnetic field, B, pointing perpendicular to the plane. The electrons follow circular cyclotron orbits that are quantised into the so-called Landau levels (LL), with energies denoted by $E_n = (n + 1/2)\hbar\omega : n \in \mathbb{Z}$ and $\omega = eB/m_e$, the well-known cyclotron frequency. When disorder is brought into the picture, the LL's are broadened by diffusive motion into a Landau band (LB), which localises all states in the bulk of the sample except for a single state which behaves critically in each band centre - a so-called *critical* state [67].

At the edge of the system, skipping electron orbits lead to the aptly-titled 'edge states'[33], which are extended states along the boundary and cause the surprising plateau structure of the phase transition in the Hall conductance [84], as illustrated in Figure 1.1. These plateaus were completely unexpected as they are a sign of stability and thus strong predictability arising from the opposite - disorder. When one tunes the Fermi energy, the energy difference between the highest and lowest occupied states, through a critical state, the system undergoes a quantised phase transition between localised phases [57]. The critical exponent, ν, describes the power law divergence of an observable called the localisation length, ξ, at the IQH

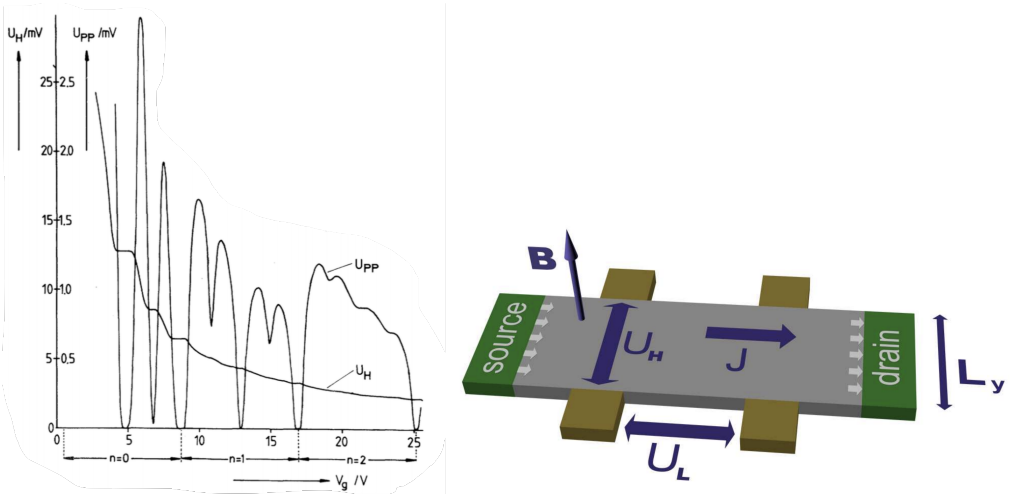

Figure 1.1: (Right) Illustration of Hall experiment setup in which an external magnetic field, **B**, induces a potential difference in the direction of the current, **J**. (Left) Experimental plot by von Klitzing of the Hall voltage versus the voltage drop between the potential probes. For specific values of the filling factor, n, there exist plateaus which contradict the classical Hall picture. The resistance on said plateaus is quantised in units of $e^2/\hbar$ as $1/n$ which is precisely the IQH effect [84].

critical point energy, E_c, as follows, $\xi \sim |E - E_c|^{-\nu}$ [26, 3, 89]. Although attempts to find the critical exponent analytically have been made, the closest values we have which map to experimental efforts thus far come from numerics-based approaches. Early on, statistically limited results employing the Chalker-Coddington (CC) network model were very promising, as they found $\nu_{\text{exp}} \sim 2.3{-}2.4$ [38, 36, 37, 54, 39, 13]. However, in the most recent and accurate numerical studies the critical exponent was found to be in the range, $\nu_{\text{CC}} \sim 2.58 - 2.6$ [78, 55, 79, 62, 63, 1, 60] when employing the CC network model [17] as well as most recently Puschmann *et al.* using a tight binding lattice model [73].

The critical exponents obtained from the above high precision analyses still differ significantly from the experimentally observed critical exponent, $\nu_{\text{exp}} \sim 2.38(5)$ [55]. Thus, one can conjecture that the CC network model does not capture the IQH transition in its entirety and what is required is the inclusion of interactions which exists in real materials [68, 70, 85, 71, 10, 55]. In this thesis, we remain in

the non-interacting regime and perform a high accuracy study with the Real Space Renormalisation Group (RSRG) approach on the CC network model. Upon investigation, we find that there exist two renormalisation group structures that produce the closest values to the IQH critical exponent as the aforementioned recently simulated results using the CC network and a tight binding model produced. The main body of the work investigates the proposition that another type of disorder must be into account - geometric disorder (GD), which first suggested by Gruzberg *et al.* in Ref. [30].

The research we will present focuses on finding a shift in the critical exponent of the IQH when taking into account GD. Its justification lies in the assumption made when considering a regular lattice: the electrons are inherently ordered in some fashion. However, in reality, their relative angles and distances are random, and when they incorporated this into the CC model [30], the authors found that for a particular amount of geometric disorder, there emerges a new critical exponent. The closeness of the value they obtained for a particular amount of GD when compared to experiment is still not well understood. For example, in the tight binding model based work by Puschmann *et al.* in Ref. [73], the authors indicate that the statistics are at fault - i.e. their numerical analysis involved a small sample set similar to the early studies and thus it is no surprise that they obtained a value for ν close to the ones obtained in early numerical studies and experimental observation - thus their results may be unreliable. However, even if the study in Ref. [30] was poorly done the validity of incorporating GD remains unchallenged.

The work in Ref. [30] employed the transfer matrix (TM) method as their numerical technique [81], and applied it to the Chalker-Coddington (CC) network model with a regular lattice structure [17], modified by GD. When including this new type of disorder at a particularly chosen 'magnitude', they claim to have discovered a value of the calculated exponent, $\nu \sim 2.3$. This leads the authors to believe that there exists either one or even a line of critical exponents which depends solely on

the magnitude of the GD imposed on the system.

The further claim is that this type of structural disorder can be taken as effective fluctuations in 2D Euclidean space-time and hence a coupling to 2D quantum gravity (2D QG) [23]. This has been previously studied and shown to modify critical exponents of statistical mechanics models. The shift of said exponents is given by the Knizhnik-Polyakov-Zamolodchikov (KPZ) relation in Ref. [50]. Thus, one can postulate that such a modification is happening in the modified CC model being studied. We aim to provide an overview of the reasoning behind this to test its justifiability.

The aim of our work, on the other hand, was to set out in finding this line of critical exponents using a different approach - the real-space renormalisation group (RSRG) method. The RSRG approach has its roots in classical percolation theory,[80] whenceforth it was then employed in Ref. [13], in finding the critical exponents of the IQH with the CC network model. The results we found employing the RSRG method have demonstrated a shift of the critical exponent upwards as GD is increased in a statistically symmetric fashion and more nuanced results when GD is varied asymmetrically. Interestingly, when investigating the results for different RG unit cell structures, we found that they not only exhibit inherent differences in their critical exponents, but there was a definite shift of their individual exponents when GD is turned on. Our paper begins by introducing the theory behind the KPZ relation and attempts to examine the method employed in modifying the CC network analytically as well as numerically to match said relation.

Chapter 2

Background and Theory

In this chapter, we will lay the necessary groundwork which was needed to develop our understanding and produce our results. We will begin by a detailed discussion of the Hall Effect, both its classical and quantised versions, elaborating on the ideas hinted at in our introduction. From there, we will introduce the theory of random networks and focus in particular on the CC network as it is the one employed in our study. Lastly, we will illustrate how 2D QG is relevant and inevitably plays a role when one attempts to formulate a purely analytical description of the IQH phenomenon.

2.1 The Quantum Hall Effect

The field of study around this and other similar phenomena began with the discovery of the Hall effect by Edwin H. Hall in 1879. This was known to be a classical result based entirely on the physics of electric and magnetic field in a conducting surface. As an instructive example one can consider the setup illustrated in Figure 1.1.

2.1.1 The Classical Case

In the setup we are considering, we have a 2D homogeneous isotropic conducting sample and an external electric field, $\mathbf{E}$, parallel to the sample. In this case, the sample acts as a resistor with $\mathbf{E} = \rho\mathbf{j}$ such that ρ is the material's resistivity and $\mathbf{j}$ is the current density. Once you turn on a magnetic field, $\mathbf{B}$, perpendicular to the sample, the charge carriers with charge, q, and velocity, $\mathbf{v}$, are deflected by the Lorentz force, $\mathbf{F} = q(\mathbf{v} \times \mathbf{B})$, which creates an additional electric field, $\mathbf{E}_H$, orthogonal to $\mathbf{E}$. The resulting force from the electric field, $\mathbf{F}_H$, leads to a corresponding Lorentz force, $\mathbf{F}_L$ and when these two forces equate, $\mathbf{F}_H = \mathbf{F}_L$, the electric field, $\mathbf{E}_H$ induces a *Hall* voltage, $U_H = L_y|\mathbf{v}||\mathbf{B}|$, such that L_y is the width of the sample [82].

One can re-write U_H using the relation, $\mathbf{j} = qn_q\mathbf{v}$ where n_q is the carrier density. It follows that,

$$U_H = \frac{1}{qn_q} L_y|\mathbf{j}||\mathbf{B}| = A_H L_y|\mathbf{j}||\mathbf{B}|, \tag{2.1}$$

where $A_H = \frac{1}{qn_q}$ is the so-called Hall coefficient, a proportionality constant which depends on the band structure of the sample's material and otherwise is independent of the experimental setup.

Since we are dealing with a 2D sample, the resistivity will be described by a tensor rather than a scalar, whence,

$$\mathbf{E} = \begin{pmatrix} \rho_{xx} & \rho_{xy} \\ -\rho_{xy} & \rho_{xx} \end{pmatrix} \mathbf{j}, \tag{2.2}$$

such that ρ_{xx} and ρ_{xy} are called the longitudinal and Hall resistivity, respectively. Conversely, the conductivity tensor is defined as the inverse of the resistivity tensor

with,

$$\sigma_{xx} = \sigma_{yy} = \frac{\rho_{xx}}{\rho_{xx}^2 + \rho_{xy}^2} \quad , \quad \sigma_{xy} = -\sigma_{yx} = -\frac{\rho_{xy}}{\rho_{xx}^2 + \rho_{xy}^2}, \tag{2.3}$$

with the analogous σ_{xx} and σ_{xy}, the longitudinal and Hall conductivity, respectively [82].

2.1.2 The Quantum Case

Let us now consider the quantum regime and how the Hall measurement is altered in this case. To do so one has to investigate the same system as described in the classical case except at very low temperatures, $< 4K$, large external magnetic field, $B > 10T$ and as thin a sample of electrons as possible to match the 2D condition. One can achieve this experimental set up in various ways, one example is placing the electrons on a free liquid helium surface which allows for very high densities [52].

The first successful measurement was achieved by von Klitzing *et al.* [84] with a Si-MOSFET at $T = 1.5K$ and $B = 18T$ which showed that if one varied the gate voltage, U_H; one observes plateaus in the Hall resistivity at quantised values, $\rho_{xy} = (1/N)h/e^2 : N \geq 1$ while $\rho_{xx} \to 0$. The measurements were also very precise, thus providing a standard candle for all resistors to be defined with respect to; this standard resistance is called the von Klitzing constant, $R_K = h/e^2$ [84]. After the seminal discovery of the IQH effect which was awarded a Nobel Prize for its importance [83], theorists scrambled to action and produced various explanations of the effect. Unfortunately, we still lack a fundamental theory for this effect, and all analytical descriptions rely on strong initial assumptions [12].

It is strongly suspected that the IQH effect is linked to Landau quantisation which provides a quantum mechanics based description of electron motion in an external magnetic field. One can start to see the effect by deploying a phenomenological approach, considering the electrons in the 2D Hall sample as free particles

moving in a magnetic field which corresponds to the following Hamiltonian,

$$\hat{H} = \frac{1}{2m^*}(\hat{\mathbf{p}} + e\mathbf{A})^2, \tag{2.4}$$

such that $\hat{\mathbf{p}}$ is the momentum operator, m^* is the effective electron mass and $\mathbf{A}$ is the vector potential which is defined by the Maxwell equation, $\nabla \times \mathbf{A} = \mathbf{B}$. Now the magnetic field causes the electrons to move along cyclotronic orbits. It is then reasonable to split the coordinates into two parts,

$$\hat{x} = \hat{X} + \hat{\zeta} \quad , \quad \hat{y} = \hat{Y} + \hat{\eta}, \tag{2.5}$$

where $(\hat{X}, \hat{Y})$ describe the position of the centre of the cyclotron motion and $(\hat{\zeta}, \hat{\eta})$ are the relative coordinates of the motion about said centre. Now we can use the Hamilton equations which provide the equations of motion from the Hamiltonian,

$$\dot{\hat{\zeta}} = -\omega_c \hat{\eta} \quad , \quad \dot{\hat{\eta}} = \omega_c \hat{\zeta}, \tag{2.6}$$

such that $\omega_c = eB/m$ is the cyclotron frequency with respect to $(\hat{\zeta}, \hat{\eta})$.

One can now re-write the Hamiltonian in equation (2.4) into in terms of $(\hat{\zeta}, \hat{\eta})$, which reduces to the familiar harmonic oscillator form,

$$H = \frac{\hbar\omega_c}{2l_B^2}\left(\hat{\zeta}^2 + \hat{\eta}^2\right), \tag{2.7}$$

such that $l_B = \sqrt{\hbar/eB}$ is the so-called cyclotron radius and defines the magnetic length scale. This is now simply a harmonic oscillator which is easy to solve for the eigen energies using the Schrodinger equation. We have thus described the so-called Landau quantisation of a free electron moving in a magnetic field and in 2D one

observes discretised eigen energies called Landau Levels (LL),

$$E_N = (N + \frac{1}{2})\hbar\omega_c, \tag{2.8}$$

where $N \geq 0$ is the LL index and corresponds to the plateaus observed by experiment.

We may now consider the differences between this model and the simple harmonic oscillator (SHO). We begin by noting that the values of $(\hat{\zeta}, \hat{\eta})$ are accompanied by an uncertainty appearing due to the commutation relation,

$$\left[\hat{\zeta}, \hat{\eta}\right] = -il_B^2. \tag{2.9}$$

Moreover, in contrast to the SHO, the Landau energy levels are degenerate. The degeneracy is physically due to electron motion at each $(\hat{\zeta}, \hat{\eta})$ being bound to a radius, l_B, implying that there exists various $(\hat{X}, \hat{Y})$ at each particular eigen energy, since their orbits do not overlap.

The degeneracy of the LL's can be quantified by a constant, N_L, which depends on l_B as well as the size $L_x \times L_y$ of the sample under consideration,

$$N_L = \frac{L_x L_y}{2\pi l_B^2}. \tag{2.10}$$

It then follows that using N_L, one can write down the filling factor, which is defined as

$$f = 2\pi l_B^2 n_e = 2\pi \frac{\hbar}{eB} n_e. \tag{2.11}$$

By definition of f, it is a dimensionless quantity that has the power to describe two experimental situations; one being the change of electron density, n_e, through varying the gate voltage and magnetic field; f, on the other hand, is expressible as the ratio of the number of electrons and the number of flux quanta, h/e, in the

sample of study. Thus, f provides one with an indication of the filling of each LL, for example, if $f = 2$, this corresponds to the lowest two levels being occupied.

The quantised energy spectrum explains the IQH transition points, but it fails to describe the regime between transition points. More specifically, why the transition between plateaus in ρ_{xy} (and consequently σ_{xy}) are observed nor the curiosity that in the same regime one observes ρ_{xx} (σ_{xx}) tend to zero. The immediate conclusion is that this model is too simplistic and one of the most significant differences between our idealised situation and reality is disorder in the sample of electrons, so maybe incorporating it will explain these phenomena.

As a result of disorder in the model, it has been shown that the LL's broaden to Landau bands (LB) as illustrated in Figure 2.1. Furthermore, another Nobel Prize winning electron model which exhibited the importance of disorder called the Anderson model of localisation [3] provides insight into the fact that not all states in each LB are extended. As is illustrated in Figure 2.1 disorder causes the states in the tails of the bands to be localised which implies that they can not contribute to charge transport. Thus, the IQH effect is comprehensible as a series of localisation-delocalisation (LD) transitions. One can note that the peak point in σ_{xx} occurs at the integer, f, where the E_F passes the extended states which lie at the centre of LB. Between the centres of the LB's states are localised and thus it must be the case that $\sigma_{xx} = 0$. On the other hand, σ_{xy} is constant while E_F is in the range of localised states and increases by e^2/h onto the next plateau after crossing the centre of an LB.

One should note that although this phenomenological approach which assumes an LD transition is highly instructive, there exist many more sophisticated theories which consider gauge invariance [51], topological quantisation [59], scattering as well as field-theoretical approaches [72] which we will be discussing further in the upcoming sections. However, until now we have not been able to write down a full description, with a Hamiltonian, which describes the IQHE in its entirety and

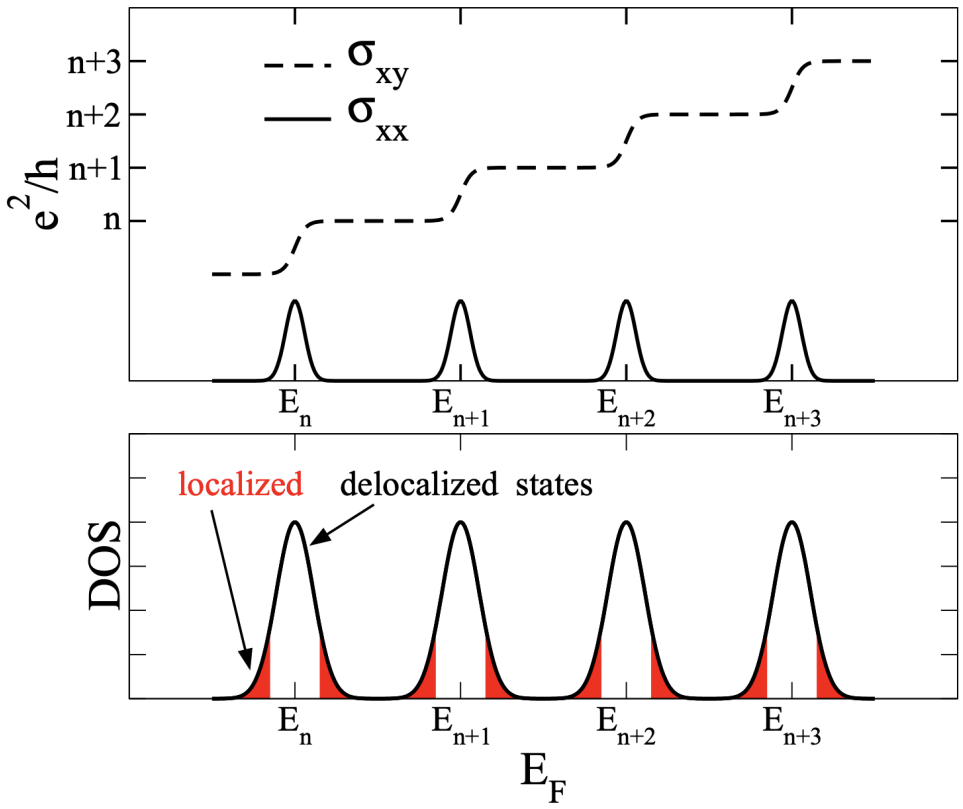

Figure 2.1: The IQH effect presented by a set of localisation-delocalisation transitions. In finite-size systems, the width of the extended states about each band centre of the Landau levels, broadened by disorder, is finite [13].

thus we must consider less straight forward but more physically realistic approaches like the CC model, which we will introduce in the next section.

2.2 The Chalker-Coddington Network Model

In our study, we will be working with and modifying a semi-classical approach to model the IQH transition. Chalker and Coddington first suggested this model in 1988 [17]. It is described by a random network and is based on the high-field model (HFM) [88]. As we previously alluded to, the CC network model is a prolifically employed tool in various studies of the IQH effect and in particular those studies

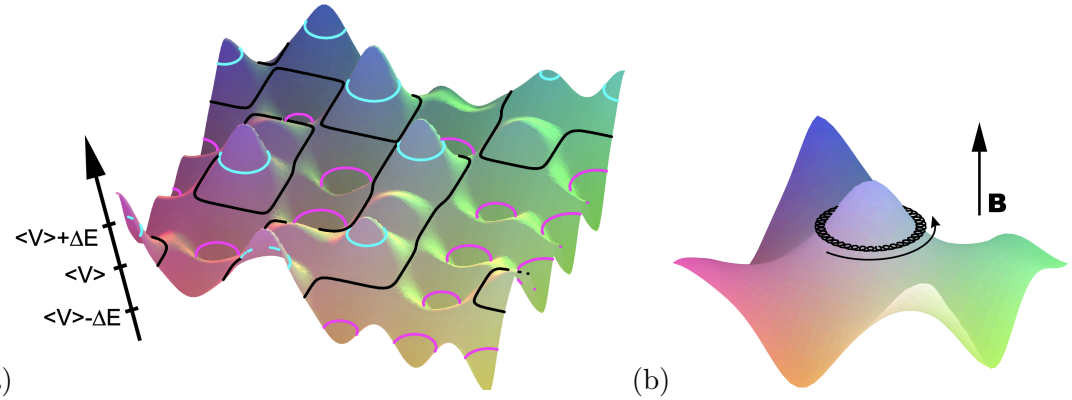

(a) (b)

Figure 2.2: (a) A 3D representation of a weakly varying random potential V with equipotential lines at $\langle V \rangle$ and $\langle V \rangle \pm \Delta E$. In a strong magnetic field, B, the electron motion is separable, illustrated by the black orbit in (b), into both cyclotron and guiding centre motion along equipotentials [13].

aiming to extract the critical exponent [38, 36, 37, 54, 39, 13, 78, 55, 79, 62, 63, 1, 60]. To incorporate the LD transitions into the HFM model two postulates are needed: firstly, the electrons do not interact with each other and instead interact through a smoothly varying potential landscape, $V(\mathbf{r})$, in 2D and secondly, the external perpendicular B field is very strong, see Figure 2.2 for an illustration. Whence, the B field forces the electron into a cyclotron orbit with radius, l_B, that is much smaller than the fluctuations of the potential [17]. Hence, one may separate the cyclic from the equipotential guiding centre motion. This cyclotronic motion leads to the desired quantisation into discrete LL's while its influence on the motion along the potential surface is negligible [88]. The model contains no explicit dependence on the magnetic field as it only contributes to the electron's phase, and thus electron transport is dictated by the height of the saddle points (SP) in $V(\mathbf{r})$ [13], as illustrated in Figure 2.3. The CC network model introduced quantum corrections - tunnelling and interference - to the HFM. From a semi-classical perspective, tunnelling takes place when electron cyclotron orbits overlap due to being too near to one another which by inspection of Figure 2.3 occurs at the SP's. This means that the SP's can be seen as quantum scatterers are describable by a unitary matrix, S, defined as

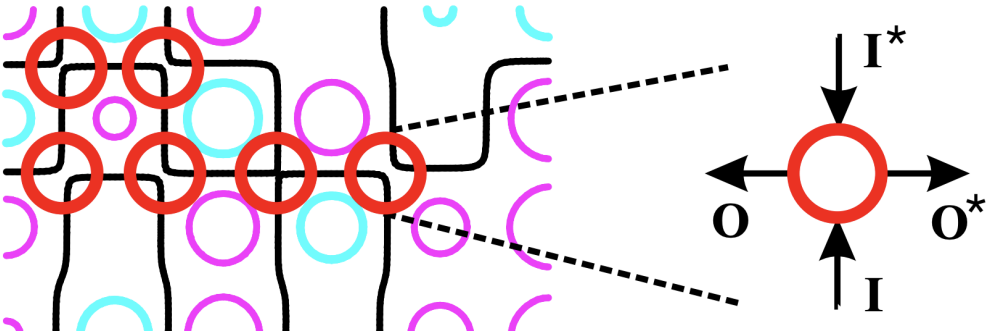

Figure 2.3: The equipotentials provide one with the SP's as indicated in this diagram. A single SP acts as an electron scattering point linking two incoming, (I, I^*), with two outgoing, (O, O^*), channels [13].

follows,

$$\begin{pmatrix} O \\ O* \end{pmatrix} = S \begin{pmatrix} I \\ I* \end{pmatrix} = \begin{pmatrix} t & r \\ -r & t \end{pmatrix} \begin{pmatrix} I \\ I* \end{pmatrix}. \tag{2.12}$$

Thus, two incoming and two outgoing channels are connected by the scattering matrix, S. We assume the potential is symmetric at each SP and the scattering rates are provided by complex transmission, t, and reflection, r, coefficients. It is clear that t and r must be dependent on the potential energy at an SP, moreover, by the unitarity of S, the following must hold, $|t|^2 + |r|^2 = 1$. Gruzberg *et al.* showed in Ref. [31] that one can parameterise the coefficients as follows,

$$t = \left(\frac{1}{e^z + 1}\right)^{\frac{1}{2}} \quad , \quad r = \left(\frac{1}{e^{-z} + 1}\right)^{\frac{1}{2}}, \tag{2.13}$$

such that z is the dimensionless difference of the electron energy, ϵ_e, and the SP potential [31]. Without loss of generality, one generally takes $\langle V \rangle = 0$, which means that in the case of $\epsilon_e = 0$, the value of z will be identical to the height of the SP. From these considerations one can then construct a network of SP's such that the SP's and equipotentials map to nodes and directed links, respectively, on a planar, regular, directed square lattice in 2D (see Figure 2.4). One more point to consider

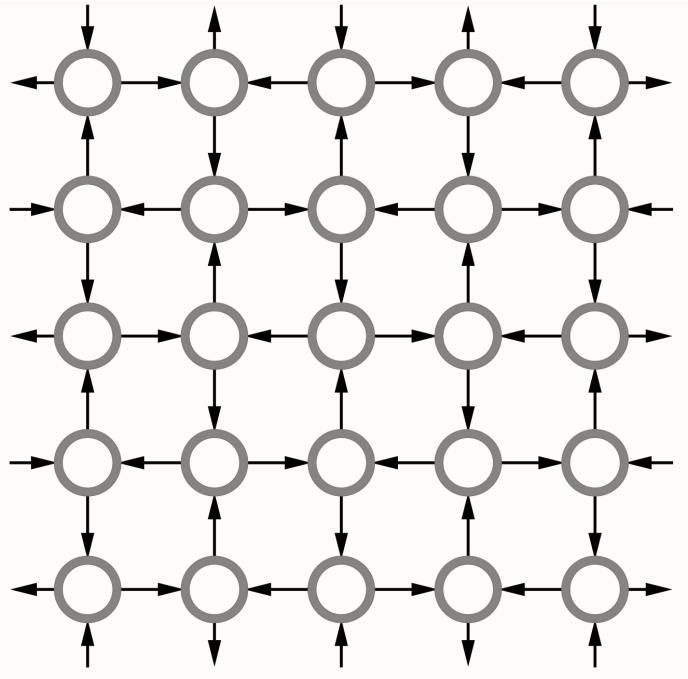

Figure 2.4: A diagram of the CC network achieved by mapping SPs to nodes and equipotentials to directed links of a regular 2D square lattice.

is that while an electron moves along an equipotential, it must pick up a phase, Φ, to model the effects of an assumed random magnetic field. The corresponding phase factor, $e^{i\Phi}$, can be included in the matrix, S, [13] or taken into account by including factors of extra diagonal matrices at each link. The CC network model , analogous to the HFM, describes a single IQH transition solely with one extended state in the centre of the LB at $\epsilon_e = 0$. One can then extract critical properties in said transition such as the critical exponent of the CC model, ν_{cc}, and check if the result aligns with experiment values of the IQH transition. More specifically, The CC model is a chiral version (due to the strong magnetic field) of a general network model [17], and may be applied to study systems lying in different so-called *universality* classes to investigate their LD transitions [9, 65]. Albeit the great success of the CC model, it is still a very simplified picture of the real world, and it is surprising that it can predict experimental results. The reason behind this immense predicting power is

based on a hypothesis called universality.

Phase transitions, such as that which is exhibited in the IQH transition, are characterised by a type of critical behaviour, for example, the emergence of length scale, l_B, which is quantifiable by a set of corresponding critical parameters. The term universality in this context is used to describe the assumption that these critical parameters are not specific to a sample in an experiment or even a theoretical model. He showed the first case of demonstrable universality in Ref. [86] with the study of statistics of nuclear spectra. Wigner found that instead of employing experimentally observed energy levels, the correlations in the spectra are reproducible as the eigenvalues of some randomly chosen matrices according to a Gaussian distribution.

With universality one then expects the quantities deemed to be universal, to be the same across a variety of systems which are similar only in their dimensionality and underlying symmetries which may be argued on physical grounds or by inspection of the Hamiltonian if one exists. In general, the symmetry classes expressed by the Hamiltonian are the Gaussian ensembles (GE) [5] which are separable into the following classes: orthogonal (GOE) with time-reversal and rotational symmetry, unitary (GUE) with intact rotational symmetry but broken time-reversal symmetry and symplectic (GSE) with time-reversal symmetry but broken rotational symmetry. In the CC model which is chiral, the strong B field breaks time-reversal symmetry, and thus it is classifiable as GUE [31].

To conclude this section, we re-iterate further that the CC model has turned out to be incredibly more useful than first expected and applies to a range of critical phenomena aside from the IQH transition. This is mainly due to its correspondence (which we will be investigating further in Section 3) with field theory and Dirac fermion models which were first demonstrated in Refs. [53, 57].

2.3 Percolation Theory and the RG Approach

In this section, we will discover that one can relate the CC model to classical percolation in a 2D square lattice. This is achieved by mapping each SP to a so-called *bond* in percolation theory [74]. To connect to the physical perspective, one considers a bond to be connected solely when the potential at the SP in question is less than or equal to the potential energy of the electron, ϵ_e at that SP.

Once this mapping to a percolation problem is achieved we will be employing an RG technique to study the CC model's critical properties. RG is one of many powerful tools to study phase transitions [87]. The first overarching quality of RG approaches is their elimination of irrelevant short range or high-frequency degrees of freedom. These quantities can be restored post calculation by some appropriately chosen scale transformation - thus the system is left with the same structure as the original one albeit with the values of its parameters (coupling constants for example) renormalised. Secondly, the RG approach is based on iteration until convergence, each iteration is called an RG step, and once convergence to the desired accuracy is attained one can extract critical properties of a transition of interest.

We will be employing the real space RG (or RSRG) approach [74] and thus will omit a discussion of field-theoretical RG techniques (for a review see Ref. [89]). RSRG is best illustrated by example, and we will consider the case of bond percolation on a 2D square lattice whose network is based on links (bonds) between nearest neighbour nodes. One then assigns a probability, $p \in [0, 1]$, to the likelihood of bonds existing between nodes which is identical throughout the network, see Figure 2.5 for an illustration of three percolation networks with different values of p. One always begins with an empty network (no bonds $p = 0$) of some size, $L \times L$, and as one increases p, more bonds are likely to appear between nodes. As p gets large, the network starts to form percolating clusters which are connected nodes which exhibit one or more unbroken paths between two opposite network borders. When

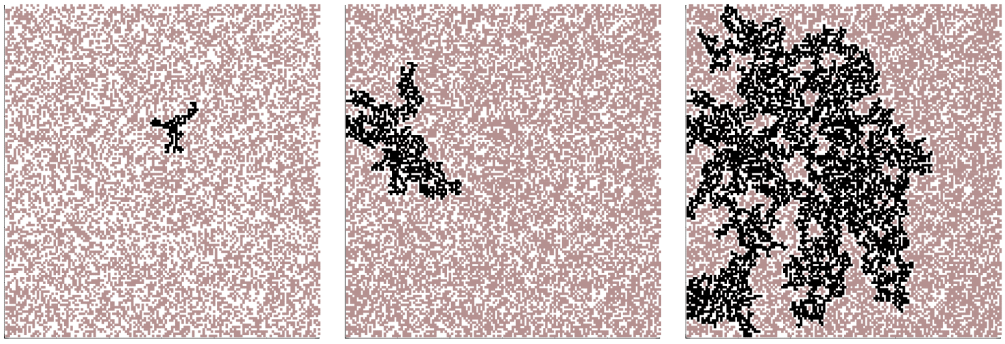

Figure 2.5: Diagrams of bond percolation networks on a 2D square lattice for various increasing bond probabilities from left to right. Black dots represent bonds and the diagram on the far right illustrates a percolating cluster which manages to connect two borders of the sample [18].

a cluster percolates we have reached a threshold probability, $p_c(L)$, and this probability defines a percolating cluster. The values of p_c will depend on the random realisation of a particular network and in the limit, $L \to \infty$, p_c attains a unique value which is sample independent with respect to a particular type of network. To obtain a high-level approximation to p_c thus seems to be a brute force, daunting, computational task but fortunately, there is another way.

The RSRG approach has been shown to allow one to approximate p_c in a computationally non-intensive way [74]. The main assumption behind the RSRG method is that a certain section of the network under consideration, called the RG unit, sufficiently represents the essential qualities of the whole network. The RG unit consists of a small number of bonds, and the RSRG approach dictates an RG transformation to replace the RG unit in the network by a so-called super bond with new probability, $\mathcal{R}(p)$, determined by the probabilities, p, of the bonds it consists of (see Figure 2.6 for an illustration). From the super bonds, with probabilities, $\mathcal{R}(p)$, one can then construct an analogous percolation network which is renormalised identically to the original network. Repeating the transformation (RG steps) allows one to obtain an accurate approximation for large samples since after each step the effective sample size grows by a factor pre-determined by the geometry of the

Figure 2.6: Illustration of the RG approach to the 2D bond percolation where the black lines and empty circles represent bonds and lattice sites, respectively. A five-bond RG unit (Left) is mapped onto a single super bond (Right).

p^5	
$p^4(1-p)$	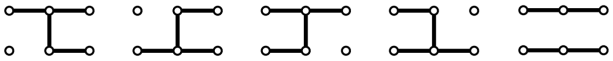
$p^3(1-p)^2$	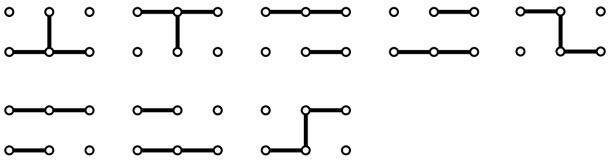
$p^2(1-p)^3$	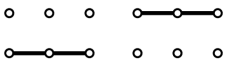

Table 2.1: A table of the set of configurations of a 2D bond RG unit labelled by the probability of them occurring [18].

original RG unit selected. Consider the example of a super bond consisting of five bonds forming the shape illustrated in Figure 2.6. The super bond probability, $\mathcal{R}(p)$, is then found by the sum over all configurations which connect the left to the right end of the chosen RG unit, as illustrated in Table 2.1 . Thus, the probability of a single configuration is the product over five bond probabilities such that a bond and a lack thereof contributes probability, p and $1-p$, respectively. We are therefore left with the following simple expression for $\mathcal{R}(p)$,

$$\mathcal{R}(p) = p^5 + 5p^4(1-p) + 8p^3(1-p)^2 + 2p^2(1-p)^3. \tag{2.14}$$

To approximate the threshold percolation probability, p_c, one requires $\mathcal{R}(p) = p = p_c$ to hold. This is called the fixed-point (FP) condition in the context of RSRG [74]. One can immediately spot trivial solutions to the FP relation, $p_c = 1, 0$, while the sole non-trivial one is $p_c = 1/2$. One can then employ this non-trivial solution to estimate the critical exponent ν_{perc}, of the correlation length of a such a percolation transition, defining a characteristic length,

$$\xi = a(p_c - p)^{-\nu_{perc}}, \tag{2.15}$$

such that a is the lattice constant of the original network under consideration. The super network must exhibit analogous behaviour but in our example of a five bond super cell it is clear that its lattice constant, $a' = 2a$, by the size of the RG unit. We can now equate the characteristic length scales, $\xi' = \xi$, to approximate ν_{perc} using $p_c = 1/2$, whence, from Eq. (2.15),

$$\nu_{perc} = \left.\frac{\log 2}{\log d\mathcal{R}(p)/dp}\right|_{p=p_c=1/2} \approx 1.43, \tag{2.16}$$

which deviates from the exact value of $\nu_{perc} = 4/3$ by a mere 7%, an impressive result for a deceivingly simple back of the envelope calculation. The subtlety in this result lies in the choice of RG unit cell and how well it describes the original network. To re-iterate, this method is by no means exact due to the full connectivity of the original network being lost, and thus the accuracy of the result must still be checked rigorously.

Next we will discuss our application of RSRG to the CC model with its quantum effects. We will see that the bond percolation example we considered here will have many similarities.

2.4 Quantum RSRG Approach

The RSRG approach applies to the CC model in an analogous fashion to its use in bond percolation. In the case of the CC model, the SP's of the network take the place of the bonds in the RG unit. The RG transformation, on the other hand, differs in that it must relate the S matrices of each SP to the S matrices of the super SP.

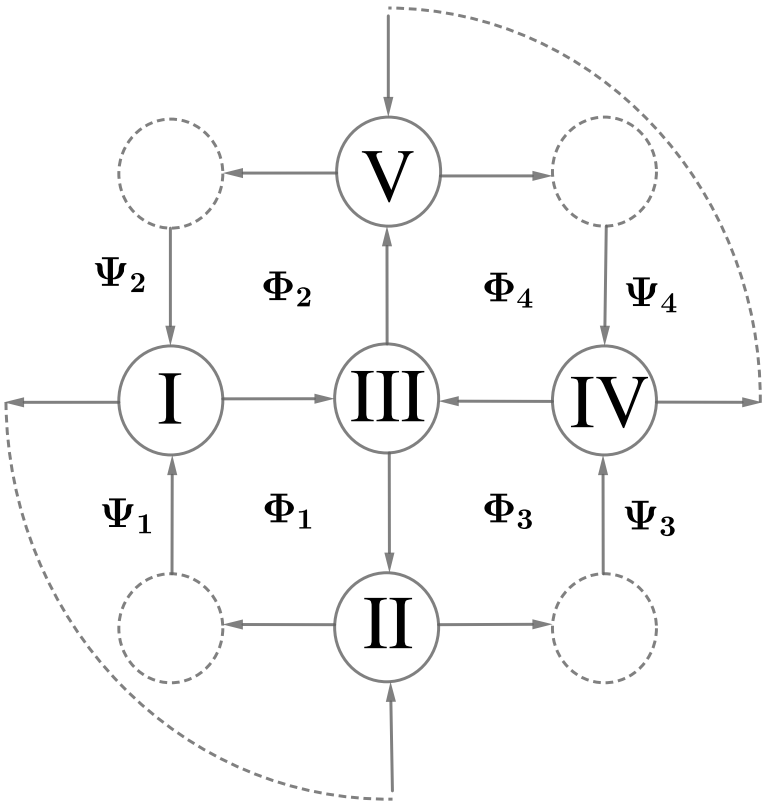

Figure 2.7: A CC network on a square lattice with nodes (circles) and links (arrows). The RG unit depicted consists of five nodes (full circles) and neglects some connectivity (dashed circles). The arrows in the diagram illustrate whether the channels are incoming or outgoing. The phases, $\Phi_1, ..., \Phi_4$, are acquired by an electron along the loops with orientation following the arrows. The wave function amplitudes, $\Psi_1, ..., \Psi_4$, are also labelled in the diagram and the curved dashed lines on the corners illustrate the chosen boundary conditions.

The super SP we will employ to illustrate the procedure, will consist of five SP's of the original network, similarly to the five bond unit studied in the percolation example studied previously. The super-SP structure to be considered is displayed in Figure 2.7, where the circles represent SP's and the lines map to links in the network. By inspection of figure 2.7, the loss of connectivity is clear when working with the super SP instead of the original network, i.e. the four edge nodes within a 3×3 section of the network are taken to be open (their bonds are neglected). This super SP structure leaves us with an identical amount of incoming and outgoing channels as each SP on the original CC square lattice. In a further analogy to the bond percolation example studied, by inspection, the size of the RG unit is $2a$ as well, where a is the lattice constant that represents a unit of lattice spacing.

In the RSRG approach, an electron travels along equipotential lines between SP's of a specific RG unit, accumulating a phase as in the original network. The phases are uncorrelated, this is meant to represent the randomness of the original potential landscape. Each SP is describable by an S matrix providing simultaneous equations that relate amplitudes of the wave function of incoming and outgoing channels, (I_i, I_i^*) and (O_i, O_i^*), respectively.

Every incoming channel, (I_i, I_i^*), besides the external inwardly directed channels, (I_1, I_4^*), are expressible in terms of outwardly directed channels, (O_i, O_i^*) using the phases, Φ_i. For example, $I_5 = e^{i\Phi_{15}} O_1$, where Φ_{15} is the phase shift along the link between SPs $\mathbb{I}$ and $\mathbb{V}$. The scattering equations which result from these relations (of which there are ten in our example) can be solved linearly to obtain the transmission coefficient of our super SP, more explicitly,

$$A\mathbf{x} = \mathbf{b}, \tag{2.17}$$

such that,

$$A = \begin{pmatrix}
1 & 0 & 0 & 0 & 0 & -e^{i\phi_{31}}r_1 & 0 & 0 & 0 & 0 \\
0 & 1 & 0 & 0 & 0 & e^{i\phi_{31}}t_1 & 0 & 0 & 0 & 0 \\
0 & -e^{i\phi_{12}}t_2 & 1 & 0 & 0 & 0 & 0 & -e^{i\phi_{42}}r_2 & 0 & 0 \\
0 & -e^{i\phi_{12}}r_2 & 0 & 1 & 0 & 0 & 0 & e^{i\phi_{42}}t_2 & 0 & 0 \\
0 & 0 & -e^{i\phi_{23}}r_3 & 0 & 1 & 0 & 0 & 0 & 0 & -e^{i\phi_{53}}t_3 \\
0 & 0 & e^{i\phi_{23}}t_3 & 0 & 0 & 1 & 0 & 0 & 0 & -e^{i\phi_{53}}r_3 \\
0 & 0 & 0 & 0 & e^{i\phi_{34}}t_4 & 0 & 1 & 0 & 0 & 0 \\
0 & 0 & 0 & 0 & -e^{i\phi_{34}}r_4 & 0 & 0 & 1 & 0 & 0 \\
-e^{i\phi_{15}}t_5 & 0 & 0 & 0 & 0 & 0 & -e^{i\phi_{45}}r_5 & 0 & 1 & 0 \\
-e^{i\phi_{15}}r_5 & 0 & 0 & 0 & 0 & 0 & e^{i\phi_{45}}t_5 & 0 & 0 & 1
\end{pmatrix},$$

$$\mathbf{x} = \{O_1 \quad O_1^* \quad O_2 \quad O_2^* \quad O_3 \quad O_3^* \quad O_4 \quad O_4^* \quad O_5 \quad O_5^*\},$$

$$\mathbf{b} = \{t_1 \quad I_1 \quad 0 \quad 0 \quad 0 \quad 0 \quad r_4 I_4^* \quad t_4 I_4^* \quad 0 \quad 0\}. \tag{2.18}$$

One can then relate the amplitudes on the external links with the amplitudes of the super SP; let $I_1 = I'$ and $O_5 = O'$, thus implying $I_4^* = I'^*$ and $O_2^* = O'^*$. Without loss of generality, one can choose the incoming links of the super SP to be $I' = 1$ and $I'^* = 0$, then the transmission coefficient, t' of the super-SP, is obtainable, since $O' = t'I' = t'1 = t'$.

Solving the matrix Eq. (2.17) yields the following expression for the super SP transmission coefficient [13],

$$t' = \left| \frac{t_1 t_5 (r_2 r_3 r_4 e^{i\Phi_3} - 1) + t_2 t_4 e^{i(\Phi_1 + \Phi_4)} (r_1 r_3 r_5 e^{-i\Phi_2} - 1) + t_3 (t_2 t_5 e^{i\Phi_1} + t_1 t_4 e^{i\Phi_4})}{(r_3 - r_2 r_4 e^{i\Phi_3})(r_3 - r_1 r_5 e^{i\Phi_2}) + (t_3 - t_4 t_5 e^{i\Phi_4})(t_3 - t_1 t_2 e^{i\Phi_1})} \right|. \tag{2.19}$$

Now one may employ Eq. (2.19) as our RG transformation, allowing one to generate a distribution of transmission coefficients of the super SP's, $P(t')$, averaged over the summed phases Φ_j. More specifically, each Φ_j represents the sum over three random phases forming a particular closed loop within an RG unit. The distribution, $P(t')$, is generated using the renormalised distribution of the transmission coefficients of the original SP's, $P(t)$.

However, recall that our original SP's transmission coefficients depend on electron energy, ϵ_e. Since delocalisation occurs at $\epsilon = 0$, this implies that there

exists a distribution, $P_c(t)$, and $P_c(t^2)$ is symmetric with respect to $t^2 = 1/2 = t_c^2$ which we can call the fixed point (FP) distribution. The distribution, $P_c(t^2) = P_c(G)$ (where $G = t^2$ is called the dimensionless conductance) can be related to $P_c(t)$, by definition of G, as follows,

$$P_c(G) \equiv \left|\frac{dt}{dG}\right| P_c(t) = \frac{1}{2t} P_c(t). \tag{2.20}$$

To obtain the critical exponent of the CC model from the above distribution, we must first use the relation between the transmission coefficient, t_i, and the dimensionless SP heights, z_i, in Eq. (2.13). The relation also holds for the transmission coefficient of the super SP, t', providing one with its height, z'. Thus one may generate a distribution, $Q(z)$, of the SP heights which can be related to $P(G)$ as follows,

$$Q(z) = P(G)\left|\frac{dG}{dz}\right| = \frac{1}{4}\cosh z/2^{-2} P[(e^z + 1)^{-1}]. \tag{2.21}$$

$Q(z)$ represents a parametrisation of the conductance distribution which, as we will show, provides a simple way to extract an approximation of the critical exponent of the CC model, ν_{cc}.

Let us begin with some initial distribution, $Q_0(z) = Q_c(z - z_0)$, which is shifted by $z_0 \propto \epsilon_e$ from the critical distribution, $Q_c(z)$. This shift in SP height can be seen as a consequence of a small increase in electron energy, as measured from the LB centre. Since the IQH transition is asymptotically peaked at $z_0 = 0$, this implies that for all $z_0 \neq 0$, each RG step will drive the initial distribution, $Q_0(z)$, further from the FP. If we take the shift to be small, $z_0 \ll 1$, the first RG step would result in the distribution, $Q_c(z - \tau z_0)$, for some $\tau \in \mathbb{R}$ independent of z_0. After n RG steps, the centre of the distribution will be shifted by $z_{max,n} = \tau^n z_0$, and the sample size will be increase by s^n, such that s is the size of the RG unit (called the scale factor), and $s = 2$ for the five SP RG unit. There exists a certain number, N,

of steps at which the shift will reach,

$$z_{max,N} = \tau^N z_0 \sim 1, \tag{2.22}$$

at which point a given SP is unlikely to transmit by inspection of the relation (2.13). At this point, the localisation length, ξ, will be equivalent to the size of the system, $s^N a$, such that a is the usual lattice constant of the original network, hence we can rewrite the above relation,

$$(\xi/a)^{(\log\tau/\log 2)} z_0 \sim 1, \tag{2.23}$$

and thus ξ will diverge as follows,

$$\xi \sim a z_0^{-(\log\tau/\log 2)} = a z_0^{-\nu_{cc}} \Rightarrow \nu_{cc} = \log s/\log\tau. \tag{2.24}$$

We identify $\log 2/log\tau = \nu_c c$ above by comparison with definition of the localisation length, ξ, at the IQH critical point energy, E_c, which has the following relation [82],

$$\xi \sim |E - E_c|^{-\nu}. \tag{2.25}$$

Re-arranging Eq. (2.24), one obtains a formula for the critical exponent with respect to $z_{max,n}$,

$$\nu_{cc} = \frac{\log s^n}{\log \frac{z_{max,n}}{z_0}}. \tag{2.26}$$

Lastly, when carrying out this procedure one should to make sure that z_0 is sufficiently small such that $z_{max,n} \propto z_0$ for n large enough.

In the upcoming section we will introduce the last ounce of background theory before discussing our methods and results; specifically, we discuss an analytic formulation of the IQH transition and its link to 2D QG.

Chapter 3

Analytical Formulation and 2D Quantum Gravity

The main purpose of this section is to argue that an ensemble of random networks (RN's) is, in the continuum limit, equivalent to a system of free Dirac fermions coupled to random potentials - analogous to the CC model - as well as 2D QG. The coupling to 2D QG has been shown to modify the critical exponents of well-known statistical mechanics models [29, 67, 69]. The suggestion is that a similar modification will happen for RN's, which can be constructed from the CC network model with an appropriate modification. This CC network modification is done by incorporating a new type of disorder called geometric disorder (GD), which can then be simulated numerically. One can study varying amounts of GD with various super cell structures to find a value for the critical exponent that matches experiment.

3.1 Random Networks

Rigorously, the RN's of interest to us are built on planar directed graphs in which every vertex has two incoming and two outgoing edges. The edges (links) of the network alternate as one goes around a vertex (node). The graphs of RN's divide

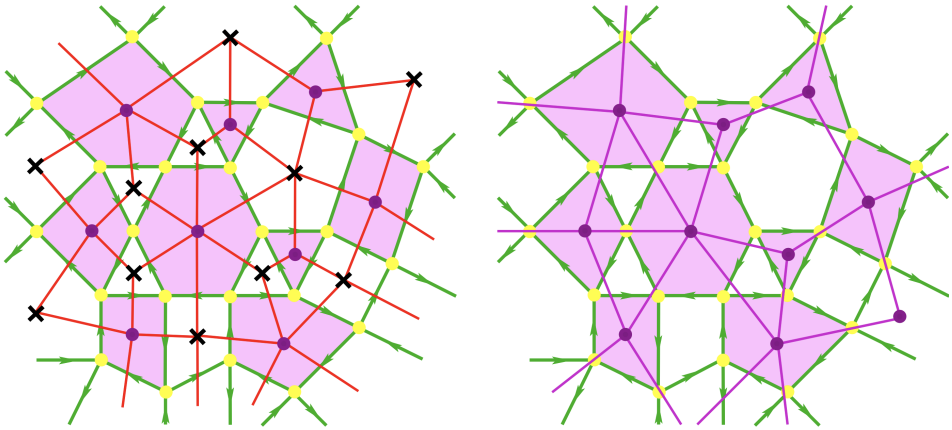

Figure 3.1: (Left) Diagram of a 2D RN and its dual. (Right) RN and its percolation lattice [30].

the plane into two sets of polygonal faces with opposite orientations of their edges as depicted by green arrows in Figure 3.1. We can represent a state of a random graph by a complex vector, $Z \in \mathbb{C}^N$, such that N is the number of edges of said graph. Each component of Z, z_e, represents the channel between a pair of nodes of an edge, e. The network model includes random scattering matrices connecting incoming, $(z_1, z_{1'})$, and outgoing, $(z_2, z_{2'})$, channels placed at the vertices. Focusing on the CC network model, one can write the familiar S matrix equation with our newly introduced notation, as illustrated in Figure 3.2,

$$\begin{pmatrix} z_2 \\ z_{2'} \end{pmatrix} = S \begin{pmatrix} z_1 \\ z_{1'} \end{pmatrix} = \begin{pmatrix} te^{i\gamma} & re^{i\gamma'} \\ re^{i\gamma} & -te^{i\gamma'} \end{pmatrix} \begin{pmatrix} z_1 \\ z_{1'} \end{pmatrix}, \tag{3.1}$$

The scattering amplitudes satisfy $t^2 + r^2 = 1$, and the scattering phases, (γ, γ'), are random.

The evolution of such a network in discrete time steps is specified by a $N \times N$ unitary matrix, U, composed of all node scattering matrices [16]. In the Feynman path integral approach to quantum mechanics [28], the Green's function of a system of interest is expressible in the supersymmetric (SUSY) formalism of random matrix

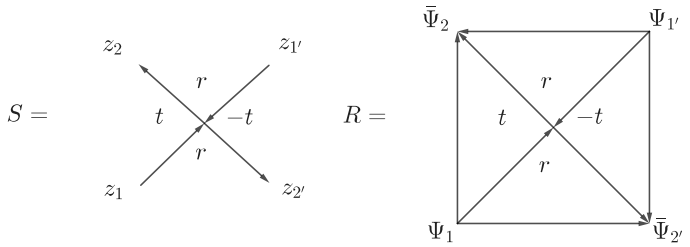

Figure 3.2: (Left) we have a diagrammatic representation of an S matrix and (Right) its corresponding R matrix.

theory as the following super integral [32],

$$G(e_1, e_2; \eta) = \int \mathcal{D}\Psi \Psi_{e_1} \overline{\Psi}_{e_2} \exp \sum_{e,e'} \overline{\Psi}_e (e^{-\eta} U - 1)_{ee'} \Psi'_e, \tag{3.2}$$

where the $e_{1,\ldots,N}$ are the usual graph edge labels and $\overline{\Psi}_e = (\overline{\phi}_e, \overline{\psi}_e)$ consist of bosonic and fermionic variables assigned to the edge labelled e (hence the SUSY moniker), as shown in Figure 3.2. The use of bosonic and fermionic variables is standard in the SUSY method and is necessary to perform disorder averages, see Ref. [44] for a review. One is free to choose the gauge parameter, η, without loss of generality, hence for the derivation that follows it is simplest to pick $\eta = 0$. One can now imagine recasting the network into a lattice by connecting the midpoint of each edge, e, 'forward' to two other midpoints by two vectors, ξ_e. These vectors form the so-called 'medial lattice' (ML) of the original random network, as shown in Figure 3.3. Whence a scattering node is replaced by a rectangle, and we get an alternative representation of the random network as a random medial lattice. By inspection of the Green's function and the unitarity of U, the action for the random network can be written as,

$$\mathcal{S} = \sum_e \overline{\Psi}_e \Psi_e - \sum_{e,v_e} t_{e,v_e} e^{i\gamma_e} \overline{\Psi}_{e+v_e} \Psi_e, \tag{3.3}$$

which represents the hopping of fermions and bosons on the random ML, and the hopping amplitudes take values r and $\pm t$ depending on the vector, v_e. The standard

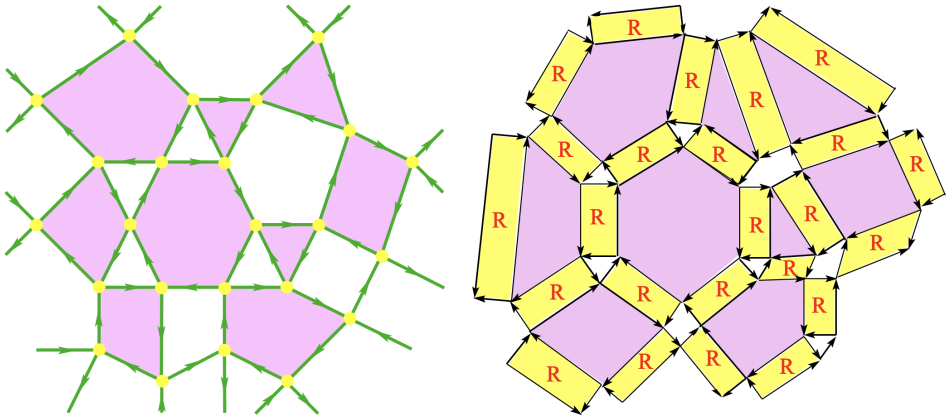

Figure 3.3: (Left) A graphical representation of a random network. (Right) The corresponding random medial lattice of the original network [30].

SUSY method is only suitable for single particle problems [43]. To this end it is necessary to use second quantisation, in which the scattering matrices at the nodes are promoted to R matrices (see Figure 3.2). These R matrices act on the Fock spaces attached to edges of the network. Given a random ML, we represent the R matrices by quadrangular faces surrounding the scattering nodes, see Figure 3.3.

The trace of the product of the R matrices over all nodes of the network provides one with the partition function [44]. In the most general case of interacting electrons, the SUSY method is no longer applicable [31]. However, in this study along with all others which attempted to find the critical exponent, we do not include such interactions and thus may continue to explore the SUSY interpretation. Thus, writing the trace of the product of the R matrices in the basis of (super) coherent states for each of the (super) Fock spaces on the edges, one obtains an identical action, S, as the previously found one in Eq. (3.5) [44].

3.2 Continuum Limits

In the case of the CC network, the ML is the square lattice with vertices labelled by some set of Cartesian coordinates, $x^a \in \mathbb{R}^2$, as shown in Figure 3.4. The vectors,

ξ_e, are $\pm\epsilon\hat{x}_a$ such that $\hat{x}_a$ are unit vectors and hence ϵ must be the lattice spacing. Near the critical point of the CC model, $t_c = r_c = 1/\sqrt{2}$ [17], the variations of the phases, γ_e, and the fields, Ψ_e, are slow, and one can cross to the continuum limit, $\epsilon \to 0$, by simply expanding the fields,

$$\Psi_{e+\epsilon\hat{x}_a} \to \Psi(x) + \epsilon\partial_a\Psi(x). \tag{3.4}$$

Moreover, re-scaling the fields in the continuum, one obtains, as in [35], the continuum action of the fields,

$$\mathcal{S} = \int d^2x\Psi \left[\sigma^\mu \left(i\overset{\leftrightarrow}{\partial}_\mu + A_\mu\right) + m\sigma^3 + V\right]\overline{\Psi}, \tag{3.5}$$

such that $\sigma^{\mu=1,2,3}$ are the usual Pauli spinors, and the symbol, $\overset{\leftrightarrow}{\partial} = (\overset{\leftarrow}{\partial} - \overset{\rightarrow}{\partial})/2$, the arrow on top of the partial indicates the direction of action, i.e. the right (left) arrow implies the operator acts on what lies to the right (left) of it. The mass term, $m \propto r - r_c$, σ^μ ,and the random gauge, $A^\mu(x)$ and scalar, $V(x)$, potentials arise as certain combinations of the random phases, $e^{i\gamma_e}$ [35].

One can now consider the random ML that is close to the square lattice as is shown in Figure 3.4. Its faces *remain* quadrangles, furthermore, one can introduce (curvilinear) coordinates, $\xi^\mu \in \mathbb{R}^2$, with respect to the vectors, v_e, in a natural way. Since physics is independent of coordinate choice, one can use either ξ^μ or x^a, as long as one remains consistent. Using the frame formalism from differential geometry to relate bases of vectors $\hat{x}_a = \mathcal{E}^\mu_a\partial/\partial\xi^\mu$ and 1-forms, $dx^a = \mathcal{E}^a_\mu d\xi^\mu$ and hence the volume element is simply, $d^2x = \mathcal{E}d^2\xi$ such that $\mathcal{E} \equiv \det\mathcal{E}^a_\mu$. The action, which is invariant under coordinate exchange can thus be re-written under change of coordinates as,

$$S = \int d^2\xi\,\mathcal{E}\Psi \left[\sigma^b e^\mu_b \left(i\overset{\leftrightarrow}{\partial}_\mu + A_\mu\right) + m\sigma^3 + V\right]\overline{\Psi}. \tag{3.6}$$

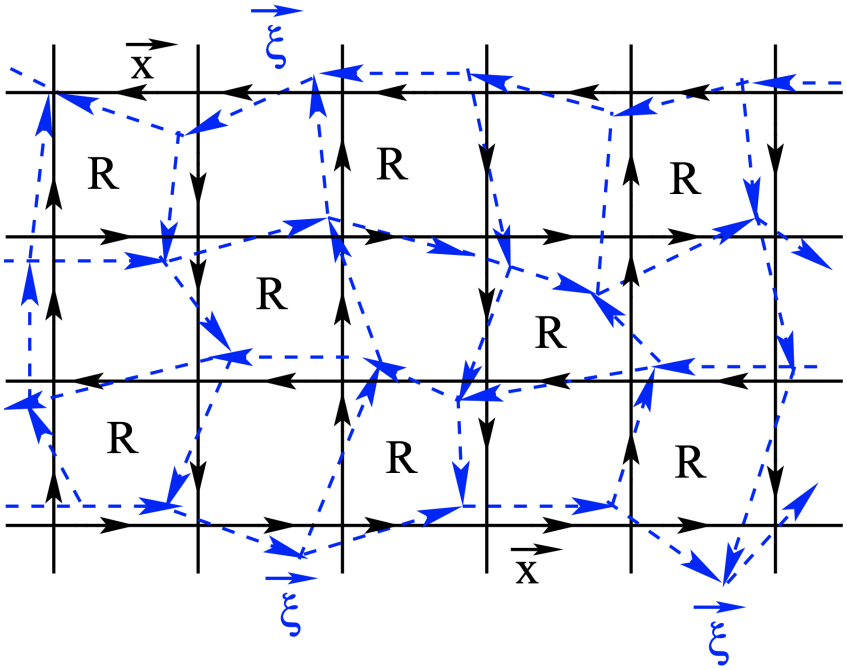

Figure 3.4: Graphical representation of weakly random medial lattice. The vertices of the original and weakly random ML are labelled by vectors, $\mathbf{x}$ and ξ, respectively [31].

This action is nearly identical to the previous one except now all terms including the mass term have a factor of $\mathcal{E}$, making the mass random as well. This term represents the now random geometry (Euclidean gravity) of the lattice. In the weakly deformed limit the random coordinate transformation matrix $\mathcal{E}$ is close to identity, implying the actions in Eq. (3.5) and Eq. (3.6) are nearly equivalent. The idea that Gruzberg *et al.* [30] propose is that random coordinate frames can account for more complicated situations as well, such as situations which correspond to *curved* surfaces represented by random graphs.

For discrete random networks in 2D, a non-zero curvature is defined by the presence of polygons with the number of sides, $n \neq 4$. We can see this simply by imagining the random quadrangulation of the plane dual to a given random network (see Figure 3.1 for illustration) and consider some n-gon within the random network which corresponds to n quadrangles meeting at a vertex of the dual quadrangulation.

Now if we try to map all quadrangles into equal squares with $\pi/2$ angles at all four corners then it is clear that connecting n such squares at a vertex creates a deficit angle of $(4-n)\pi/2$, distorting the surface of the network into a 'cone' (positive curvature) if $n < 4$ or a 'saddle point' (negative curvature) if $n > 4$.

In the continuum, on a curved surface, one defines frames and coordinates locally on a specific chart (see Ref. [58] for a review on differential geometry). When charts overlap, different coordinate systems overlap resulting in different expressions for the action. However, as we mentioned earlier, the action is always invariant under any coordinate transformations, $\tilde{\xi} = f_a(\xi^1, \xi^2)$. Hence, either way, the action is given by Eq. (3.6), but now we must consider arbitrary frame configurations and average over them. The measure on such random surfaces is assumed to be determined uniquely by the requirements of conformal and diffeomorphic invariance, see Ref. [66] for more details.

One then needs to average observables over the random geometry which can be considered as a coupling to *quenched* QG [50]. It is well-known that 2D QG modifies critical exponents of a conformal field theory (CFT) located on a fluctuating surface, an overview is or in Ref. [21]. This modification, which is given by Knizhnik-Polyakov-Zamolodchikov (KPZ) relations [50], occurs because models coupled to gravity have larger coordinate re-parametrisation symmetry than models in flat space [58]. When the central charge, $c = 0$ [23], in for example, the Anderson transitions and critical percolation (present case) [6], the relation is as follows,

$$\Delta' = \frac{1}{2}(\sqrt{1 + 12\Delta_0} - 1), \tag{3.7}$$

such that Δ_0 and Δ are scaling dimensions of operators on a flat and fluctuating surface, respectively. By replacing Δ_0 with ν_{cc} in Eq. (3.7) one can see that the RHS is smaller and to be more specific, since the most accurate recent studies found $\nu_{cc} \sim 2.58-2.6$, then the RHS gives $\nu' \sim 2.32-2.34$ which is very close to $\nu_{\rm exp} \sim 2.3$.

However, whether the KPZ relation is either partially or fully complicit in explaining the difference between the simulated and experimentally observed values of the exponent has yet to be proven.

3.3 The KPZ Relation

Although we have mentioned the KPZ relation, it is useful to derive it providing us more context on its strength as well as limitations. Although we will be presenting a physicists derivation of the geometrically well-defined relation, there exist many other ways to produce it, and we refer the reader to Refs. [23, 50, 2].

The KPZ equations demonstrate a deep relationship between the conformal weights of field operators, Δ^0, in a given 2D CFT to the scaling dimensions, Δ, of said operators when the CFT has been coupled to 2D QG. The complete relations are as follows,

$$\Delta^0 = \Delta + \frac{\gamma^2}{4}\Delta(\Delta - 1) \quad , \quad \gamma = \sqrt{\frac{25-c}{6}} - \sqrt{\frac{1-c}{6}}. \tag{3.8}$$

The first derivation of the KPZ relations by Khizhnik *et al.*[50] was done in a geometric framework by performing 2D QG in a well-chosen gauge. The scaling dimensions, Δ, then arise as weights of the $SL(2,\mathbb{R})$ when the study was done in an effective theory framework [23].

More specifically, one must consider the scaling behaviour of correlation functions in the quantum CFT plus gravity to obtain Δ. Many CFT's can be constructed from 2D statistical mechanics models when they are expressed as random geometrical objects on the plane and the scaling limit is taken [41]. This has been achieved for random walk models with interactions [24], percolation clusters [15], interface models [40], travelling salesman problems [42] and so on [41]. The scaling operators have physical meaning and are viewable as geometrical objects arising in physical models (cluster boundaries or defect lines for example). Conformal weights, Δ^0, on

the other hand, can be related to the multi-fractal dimensions of said geometrical objects [23]. The statistical models can, in general, be constructed on a random lattice, where Δ is associated with the scaling dimension of the geometrical objects expressed in this random geometry. Before we begin the derivation, it is important to note that this is the most physically based, least rigorous derivation of the KPZ relations [19]; however, it will still employ CFT techniques which requires introductory knowledge in quantum field theory (QFT), basic differential geometry and measure theory.

We begin the derivation in the complex plane with a fractal set, X, with fractal dimension, $d_H = 2 - 2x$, for some $x \ll 1$. As in many QFT problems, we must incorporate a large distance infrared (IR) regulator, to be able to do so we let X lie in a compact domain, $D \subset \mathbb{R}^2$. Next, we consider a flat measure, $d\mu(z) = dz$, on $\mathbb{R}^2$ which induces a measure on X, $d\mu_X(z)$, with dimension, d_H. One constructs this measure by approximating X with some large covering, X_ϵ, made up of circles of radius ϵ. One then defines $d\mu_X$ to be the limit of the flat measure confined to X_ϵ and rescaled by a factor, ϵ^{-d_H}. Thus, if one picks a point, $z_0 \in X$, then measures the volume of X in a disc of radius, r, centred at z_0, this volume scales, if $r \ll 1$, as,

$$V_X(z_0, r) = \int_{|z-z_0|\leq r} d\mu_X(z) \approx (r^2)^{1-x}. \tag{3.9}$$

Let us then be practical and work with the setup of a smooth conformal Riemannian metric, $g(z) = e^{\gamma\phi_0(z)}\mathbf{1}_{2\times 2}$, in a 2D plane, such that $\phi_0(z)$ is a continuous function and $\gamma > 0$. The measure on said plane is $d\mu^{\phi_0}(z) = dze^{\gamma\phi_0(z)}$ and thus, the induced measure on X, the fractal set, is,

$$d\mu_X^{\phi_0}(z) = d\mu_X(z)e^{\gamma(1-x)\phi_0(z)}. \tag{3.10}$$

The measure remains local and thus the metric can be taken to be (locally) *constant* and the scaling of volume as shown in Eq. (3.9) will of course remain valid. We

may now extend the above setup to the quantum scenario in which the metric, $g(z)$, is promoted to a random variable. The metric will retain the form, $e^{\gamma\phi(z)}$, with the requirement that $\phi(z)$ is no longer constant, but a random free field that is massless. Moreover, the measure, $d\mu_X^\phi(z)$, is upgraded to a random measure with support on X, and our goal is to calculate this measure and its quantum dimension, $d_H^Q = 2 - 2\Delta$, where Δ will surely differ from the classical value of x. The smooth function, $\phi(z)$, is taken to fluctuate at some small distance scale, $a \ll \epsilon$, which is much smaller than the regulator ϵ used to define the measure and its dimension, so the limit to take will be, $a \to 0$, first and then $\epsilon \to 0$. Thus, our quantum measure which has scaling dimension Δ, given that it remains local, will be,

$$d\mu_X^\phi(z) \propto d\mu_X(z) e^{\gamma(1-\Delta)\phi(z)}. \tag{3.11}$$

Thus, we have an ansatz and which we can employ to find Δ, we will achieve this with a self-consistency scaling argument. We begin by extending the scaling for the volume of X in a disk of radius, r, as expressed in Eq. (3.9), and replace the exponent, $d_H = 2 - 2x$, by $d_H^Q = 2 - 2\Delta$. Moreover, we must provide a covariant definition of a disk of size r around z_0, specifically we must consider the geodesic disk, $B_{z_0,r} = \{z; d_{\phi_0}(z, z_0) \leq r\}$ where $d_{\phi_0}(z, z_0)$ is the geodesic distance on our non-constant metric, g. This definition is troubling in our case as our metric is random, to use this definition we must further define a neighbourhood of z_0 as a domain which is filled by some diffusion process at 'time', $t = r^2$. This is achievable by the use of a *heat kernel* in our random metric, g.

Let us begin our calculation, as usual, by looking at the simple classical case of a (non-fluctuating) smooth metric, and hence a smooth field, $\phi_0(z)$. The heat kernel, $K^{\phi_0}(z, z_0; t)$, is then defined as the kernel of the exponentiated Laplacian,

$$K^{\phi_0}(z, z'; t) = \langle z | \, e^{t\Delta^{\phi_0}} \, | z' \rangle \,, \tag{3.12}$$

such that $\Delta_z^{\phi_0}$ is the so-called Laplace-beltrami operator [41], in our metric, g,

$$\Delta_z^{\phi_0} = e^{-\gamma\phi_0(z)}\Delta_z \quad , \quad \Delta_z = 4\frac{\partial}{\partial z}\frac{\partial}{\partial z}. \tag{3.13}$$

Now, $K^{\phi_0}(z, z_0; t)$, is a function of z whose image, at short times, t, lies in a region of size $r = \sqrt{t}$, about z_0. In flat space, $\phi_0(z) = 0$, the heat kernel is simply,

$$K^0(z, z'; t) = \frac{1}{4\pi t}\exp\left(-\frac{|z - z'|^2}{4t}\right). \tag{3.14}$$

We now consider the behaviour of the fractal measure, $d\mu_X^{\phi_0}$, at short distances by studying its convolution with our heat kernel, i.e. we take the average integral,

$$B_X^{\phi_0}(z_0, t) = \int_D d\mu_X^{\phi_0}(z)K^{\phi_0}(z, z_0; t), \tag{3.15}$$

where, as one can recall, D is some large subset of the plane. It is now appropriate to employ a Mellin-Barnes (MB) transform [64] of B_X, to study its small t behaviour,

$$M_X^{\phi_0}(z_0, s) = \int_0^\infty dt t^{s-1}B_X^{\phi_0}(z_0, t) = \int_D d\mu_X^{\phi_0}(z)M^{\phi_0}(z, z_0; s), \tag{3.16}$$

with $M^{\phi_0}(z, z_0; s)$ the MB transform of the heat kernel, $K^{\phi_0}(z, z_0; t)$,

$$M^{\phi_0}(z, z'; s) = \Gamma(s)\left\langle z\right|\left(-1/\Delta_z^{\phi_0}\right)^s\left|z'\right\rangle. \tag{3.17}$$

Thus, at short distances on a smooth metric, $M^{\phi_0}(z, z'; s)$ will behave as in the flat space case,

$$\lim_{z\to z'} M^{\phi_0}(z, z'; s) \approx M^0(z - z'; s) = \Gamma(s)\left\langle z\right|\left(-1/\Delta_z^{\phi_0}\right)^s\left|z'\right\rangle \approx |z - z'|^{2s-2}. \tag{3.18}$$

Hence, the MB transform of Eq. (3.16) behaves at small distances, $z \to z_0$, as

$$\int d\mu_X(z)|z - z_0|^{2s-2}. \tag{3.19}$$

Moreover, the fractal measure's short distance behaviour, $d\mu_X$, given by the volume, (3.9), implies that the MB transform will be convergent for $s > x$, and thus, $M_X^{\phi_0}(z_0, s)$ will be holomorphic for $\Re(s) > x$. There also exists a pole (or singularity) at $s = x$. One can then employ the inverse MB transform [64] to obtain the original function as $t \to 0$ which is,

$$B_X^{\phi_0}(z_0, t) \approx t^{-x}, \tag{3.20}$$

as expected and as occurs in the case of flat space.

We may once again extend our above arguments to the more nuanced quantum case in which $\phi(z)$ is a random free field, which corresponds to the so-called Louiville model [23]. One can consider Hamilton's action for ϕ which is normalised for convenience,

$$S = \frac{1}{4\pi} \int dz(\nabla\phi(z))^2. \tag{3.21}$$

Hence the covariance matrix (or propagator) at short distances is simply,

$$\langle \phi(z)\phi(z') \rangle = G_0(z, z') \approx -\log|z - z'|, \tag{3.22}$$

and γ, the coupling constant in our random metric, $g = e^{\gamma\phi_0 z}\mathbf{1}_{2\times 2}$ is $0 \leq \gamma \leq 2$. There will exist an ultraviolet (UV) - or short distance - divergence in calculations employing such a metric [19]. The divergences of the metric and measures can be dealt with by multiplicative renormalisation in the usual fashion [2].

As previously argued, our measure, $d\mu_X^{\phi}(z)$, on the fractal set, X, will be a random measure, locally correlated with ϕ, and be of the form of Eq. (3.11).

The measure's dimension is then modified by the fluctuations of the metric at short distance and thus as we previously claimed, $\Delta \neq x$. The quantum ϕ average of our fractal measure around z_0 is then defined as,

$$B_X^Q(z_0,t) = \left\langle \int_D d\mu_X^\phi(z) K^\phi(z,z_0;t) \right\rangle_\phi , \tag{3.23}$$

which is performed in practice trivially by empoying Wick's Theorem [41]. We may find the quantum scaling exponent, Δ, for X by perceiving that B_X^Q will approximately obey the short time, $t \to 0$, self-consistent scaling,

$$B_X^Q(z_0,t) \approx t^{-\Delta}. \tag{3.24}$$

As before we take the MB transform of $B_X^Q(z_0,t)$, which reads,

$$M_X^Q(z_0,s) = \left\langle \int_D d\mu_X^\phi(z) M^\phi(z,z_0;s) \right\rangle_\phi = \Gamma(s) \int_D d\mu_X(z) \langle e^{\gamma(1-\Delta)\phi(z)} M^\phi(z,z_0;s) \rangle_\phi . \tag{3.25}$$

Where $\Gamma(s)$ is some continuous function but there exists a pole in s arising from the UV behaviour of our integrand. One can then make the following claim for the form of the integrand,

$$\langle e^{\gamma(1-\Delta)\phi(z)} M^\phi(z,z_0;s) \rangle_\phi \propto |z-z_0|^{2s-2+(\gamma^2/2)(s-1)(2\Delta-s)}. \tag{3.26}$$

To show that the integrand indeed has this form, we begin with the following, one can write,

$$e^{\gamma)(1-\Delta)\phi(z)} M^\phi(z,z_0;s) = e^{\gamma(1-\Delta)\phi(z)} \langle z| \left(\frac{-1}{\Delta_z^\phi} \right)^s |z_0\rangle . \tag{3.27}$$

Thus one can employ the standard replica trick [41] from CFT to obtain Eq. (3.26). More specifically, we study Eq. (3.27) at $s > 0$ and analytically continue to $0 < s < 1$. Assuming $s \in \mathbb{Z}$ we use Eq. (3.27) to write the covariance matrix (the Laplacian's

inverse) as $(-\Delta_z^{\phi})^{-1} = (-\Delta_z)^{-1} e^{\gamma\phi}$ allowing us to re-write the RHS of Eq. (3.27) as,

$$\int\int dz_1 \cdots dz_{s-1} e^{\gamma(1-\Delta_z)\phi(z)} \langle z| \frac{-1}{\Delta_z} |z_{s-1}\rangle e^{\gamma\phi(z_{s-1})} \cdots e^{\gamma\phi(z_1)} \langle z_1| \frac{-1}{\Delta_z} |z_0\rangle , \quad (3.28)$$

such that $\langle z| (-\Delta_z)^{-1} |z'\rangle$ is the massless covariance matrix in flat space. One can then perform the quantum ϕ average which reads - at short distances - as,

$$\langle e^{\gamma(1-\Delta)\phi(z)} e^{\gamma\phi(z_{s-1})} \cdots e^{\gamma\phi(z_1)} \rangle \propto \prod_j = 1^{s-1} |z - z_j|^{-\gamma^2(1-\Delta)} \prod_{0<i<j<s} |z - z_j|^{-\gamma^2}. \quad (3.29)$$

We need to understand the singular part in the $z \to z_0$ expansion of Eq. (3.28) which originates from the regime where all $|z_j - z_0|$ are of the order $|z - z_0|$ since this provides us with, post analytic continuation to $0 < s < 1$, the dominant contribution. The RHS of Eq. (3.29) is of z-dimension, $-\gamma^2[(1-\Delta)(s-1) + (s-1)(s-2)/2]$,and by counting powers one obtains Eq. (3.26), as required. Moreover, the logarithms appearing in the covariance matrix do not alter this scaling, and solely provide a global factor, $\log|z - z_0|$ for $s \in \mathbb{Z}$ [41].

Now, by inspection, if one compares Eqs. (3.26) and (3.18) as well as Eqs. (3.25) and (3.19), it is clear that the first singularity of $M_X^Q(z_0, s)$ occurs at s_c and is given by,

$$2x - 2 = 2s_c - 2 + \frac{\gamma^2}{2}(s_c - 1)(2\Delta - s_c). \quad (3.30)$$

Lastly, the consistency condition, $s_c = \Delta$ implies,

$$x = \Delta + \frac{\gamma^2}{4}\Delta(\Delta - 1). \quad (3.31)$$

As required, we derived the KPZ relation employed in our study following the presentation in [19]. We employed heat kernel methods [22] which are natural as the heat kernel is the solution of a diffusion equation whose properties are simple under

conformal transformations. In particular, the heat kernel's short distance and time behaviours are connected to the spectral dimension, d_s, of the space under consideration, which for 2D QG, is known to be $d_s = 2$ [23]. The situation is thought to be very curious when dealing with intrinsic quantum Hausdorff dimension [2], which is known to be $d_H^Q = 4$ in the case of $c = 0$ ($\gamma = 8/3$), but in the general case is very difficult to study.

It is worth emphasising that although our derivation was not rigorous, the KPZ relations have been derived in various ways and are known geometrically true, moreover they have been applied to various exactly solvable statistical mechanics models [23]. In our case with the CC model, we take the central charge to be $c = 0$, as in the case for the Anderson transition [2] and there exist arguments as to why this may be the case, see Ref. [7] for such an argument.

Chapter 4

Algorithm and Numerical Techniques

In this chapter, we will be discussing the numerical techniques used in our and other studies applied to the CC random network model. We begin by briefly reviewing the often used TM method which was employed by many authors who attempt to extract the critical exponent of the IQH. This includes Gruzberg *et al.* in their initial study of the effect of GD on the said exponent. We will then go on to describe the numerical technique we used in our study, the RSRG approach, and provide a small introduction into percolation theory as it is the basis of this approach.

4.1 Geometric Disorder Algorithm

To simulate random networks numerically, instead of simply employing the CC model, we begin with the regular CC network and then modify it geometrically by focusing on each node and setting $t = 0$ with probability, p_0, $t = 1$ with probability, p_1, and leaving the node unchanged with probability $p = 1 - p_0 - p_1$. The modified nodes with $t = 0$ ($t = 1$) are open in the horizontal (vertical) direction, and opening a node changes its corresponding four adjacent square faces into two triangles and one

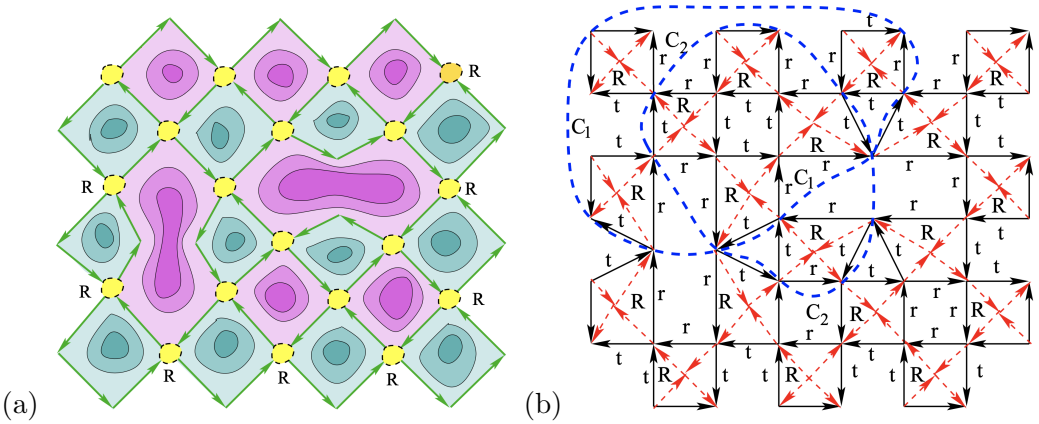

Figure 4.1: (a) Modified CC network with two 'open' nodes in both the horizontal and vertical directions, respectively. The labels R indicate the resulting R matrices from the network. (b) The corresponding ML of the modified CC network in (a). The labels t and r are the transmission and reflection coefficients at each node which will be modified by the GD [30].

hexagon as illustrated in Figure 4.1 (a) and the corresponding ML in (b). Repeated opening of nodes can produce tilings of the plane by polygons with arbitrary numbers of sides which is precisely what we define as geometric disorder. At the same time, this construction still allows for the use of the RSRG and TM methods of the CC model, but with modified t and r amplitudes. To maintain statistical isotropy of the model, i.e. an equal number on average of closed and open nodes, one sets $p_0 = p_1 = p_c$. Then one expects that the critical point is still given by the value $t^{*2} = 1/2$ for the unaltered nodes. On the other hand, the investigation of the critical exponent with broken statistical isotropy is achieved in two ways. The first method is by setting one of the $p_{0,1}$ to be zero and varying the other. The second is letting $p_0 = p_1 = p_c$ but investigating RG cell structures with a significant number of open nodes per cell.

4.2 Geometric Disorder in 2D Percolation

As the CC model is derivable as a semi-classical extension of bond percolation theory (BPT) on a 2D square lattice [17], it is useful to consider the effect of the proposed GD modification on the critical exponents of BPT and compare it to the effect on our transmission coefficients, t'. As we previously mentioned, the KPZ relation applies to classical percolation theory as well and thus we will observe how the value of the critical exponent shifts.

When it comes to picking super RG cells in classical BPT and comparing critical exponents, the best approximation obtained thus far for the BPT critical exponent, $\nu = 4/3$, is given by the symmetric five bond result [20], $\nu_5 = 1.427$, which maps to the five SP structure we discussed previously for the CC model. If one increases the size of the unit cell from five bonds in classical BPT this will result in poorer approximations to the actual exponent as opposed to site percolation [11], in which the opposite is true. Moreover, the trend for RG cell size is non-monotonic but fluctuates significantly as can be seen in [74].

As we discussed previously in section 2.3, the way one calculates the critical exponent in classical BPT with the RSRG approach is by exploring all the possible ways through the superstructure with every possible number of open and closed bonds [34], this then provides one with a unique characteristic polynomial for each RG structure. In the five bond example, we expand the polynomial in Eq. (2.14) for $\mathcal{R}(p)$,

$$\mathcal{R}(p) = 2p^5 - 5p^4 + 2p^3 + 2p^2, \tag{4.1}$$

such that $p \in [0, 1]$. From this polynomial one can obtain the critical exponent in two simple steps, the expression for the critical exponent in classical BPT is as follows,

$$\nu = \frac{\log(s)}{\log\left(\frac{d\mathcal{R}(p)}{dp}|_{p=p^*}\right)}, \tag{4.2}$$

where s is the usual scale factor and $s = 2$ for the 5 bond cell, p^* is the critical probability obtained from equating the characteristic polynomial, $\mathcal{R}(p)$, to p and finding the non-trivial, $p^* \neq \{0, 1\}$, real solutions. In our example, we have shown in section 2.3 that $p^* = 1/2$ and $\frac{d\mathcal{R}(p)}{dp}|_{p=p^*=1/2} = 13/8 \Rightarrow \nu = 4/3$.

Now we can modify the network geometrically in the same way as the CC network. Let us begin by defining a modified $\mathcal{R}$,

$$\mathcal{R}_{\text{mod}}(p, r; l_{0,1}) = \begin{cases} 0, & 0 \leq r < l_0 \\ 1, & l_0 \leq r < l_1 \\ \mathcal{R}(p), & l_1 \leq r < 1 \end{cases}, \tag{4.3}$$

where $r \in [0, 1]$ is a uniformly distributed random variable, $l_{0,1} \in [0, 1]$ is a chosen parameter which corresponds to $p_{0,1}$ in the CC model (with no imposition of statistical isotropy), and θ is the Heaviside function. It then follows that,

$$\mathcal{R}_{\text{mod}} = \tau_0 + \mathcal{R}(p)\tau_1 : \begin{cases} \tau_0 = \theta(r - l_0) - \theta(r - l_1) \\ \tau_1 = \theta(r - l_1) - \theta(r - 1) \end{cases}, \tag{4.4}$$

Now, the critical probability, $p^* = (0, 1, 1/2)$, is re-writable for clarity as, $p^* = x + \frac{y}{2}$, for some $(x, y) \in \{0, 1\}$. Plugging p^* into $\frac{d\mathcal{R}_{mod}}{dp}$, one obtains ν_{mod},

$$\frac{d\mathcal{R}_{\text{mod}}}{dp}|_{p=p^*} = \frac{13}{8}\tau_1 \Rightarrow \nu_{\text{mod}} = \frac{\log(2)}{\log(13/8) + \log(\tau_1)}. \tag{4.5}$$

Hence, τ_0 is cancelled from the expression and one is left with $\tau_1 = \{0, 1\}$, by definition, and $\log(\tau_1) = \{-\infty, 0\}$. Thus, if one increases the role played by $l_{0,1}$, this will trivially increase the number of times $y = 0$ on average and thus the number of times $\nu_{\text{mod}} = 0$. Hence, if we consider the mean value of ν_{mod} to be an approximation of the critical exponent for the case of BPT with geometric disorder, it is clear that $\langle \nu_{\text{mod}} \rangle < \nu$.

It is worth noting that x is eliminated with every unit cell structure and corresponding characteristic polynomial we have attempted, and we postulate that it is always the case in BPT. On the other hand, although in classical BPT the above result indicates an overall decrease in ν_{mod}, one can also employ the same analytical procedure for the super transmission coefficients, t', in the CC model. By mapping the arguments, $t_i \mapsto \tau_0 + \tau_1 t_i$, of the coefficients, $t'(t_i)$, one finds that in our analytic expressions for t', that firstly, τ_0 does not cancel, and secondly, there are a large number of different phase factors remaining when $\tau_1 = 0$. Hence, the situation is not as clear, and one cannot claim which way the exponent goes when $p_{0,1} > 0$. Instead we are forced to compute the results numerically as we have done in our study.

4.3 Transfer Matrix Method

The most recent and extensive study applying the TM numerical method [79], arrived at a value of $\nu_{cc} \approx 2.6$ which is significantly different from $\nu_{\text{exp}} \sim 2.3$. This motivates the inclusion of structural disorder which was also done using the TM method in the original GD study [30]. The TM formalism, first developed in Ref. [56] requires one to construct a regular 2D lattice out of the SP's of the network model. From there one cuts the 2D plane into 1D slices of length, L, with the associated scattering matrices transformed into so-called transfer matrices, T_L [81]. To illustrate, let us consider the calculation of the critical exponent of the CC model. One begins by computing the product,

$$T_L = \prod_{j=1}^{L} M_1 U_{1j} M_2 U_{2J}, \tag{4.6}$$

of layers of transfer matrices, $M_1 U_{1j} M_2 U_{2J}$ rcorresponding to two columns, M_1 and M_2, of vertical 2×2 scattering nodes,

$$M_1 = \begin{bmatrix} B^1 & & \\ & \ddots & \\ & & B^1 \end{bmatrix} \quad , \quad M_2 = \begin{bmatrix} B^2_{22} & 0 & 0 & \cdots & B^2_{21} \\ 0 & B^2 & 0 & \cdots & 0 \\ \vdots & \vdots & \ddots & \vdots & \vdots \\ 0 & \cdots & 0 & B^2 & 0 \\ B^2_{12} & 0 & \cdots & 0 & B^2_{11} \end{bmatrix}.$$

such that the elements, $B^{1,2}$, are defined as follows,

$$B^1 = \begin{bmatrix} 1/t & r/t \\ r/t & 1/t \end{bmatrix} \quad \text{and} \quad B^2 = \begin{bmatrix} 1/r & t/r \\ t/r & 1/r \end{bmatrix}, \tag{4.7}$$

and the U-matrices have a simple diagonal form with independent phase factors, $U_{nm} = e^{i\alpha_n}\delta_{nm}$. The phases, α_n, are uniformly distributed random variables in the range, $[0, 2\pi)$, reflecting the fact that the phase of an electron approaching a saddle point of the random potential is arbitrary. The scaling behaviour of the Lyapunov exponent [45], γ, near the critical point should have a finite size dependence,

$$\gamma M = \Gamma(M^{1/\nu} u_0, M^y u_1), \tag{4.8}$$

where Γ is the scaling function defined in [45], M is the number of 2×2 blocks in the transfer matrices, $u_0(x)$ and $u_1(x)$ are the relevant and irrelevant fields, respectively. The left hand side is found numerically since the Lyapunov exponent is the smallest positive eigenvalue of the following [45],

$$\lim_{L \to \infty} \frac{\log T_L T_L^\dagger}{2L}. \tag{4.9}$$

On the other hand, the right-hand side is expanded as a power series in x and powers of the lattice width, M. Re-arranging the left and right-hand side results in the critical exponent, ν [78].

4.4 Numerical RSRG implementation

We will now discuss our implementation of the RSRG approach for a range of RG unit cells. The super SP structure in Figure 4.2 (a) is our familiar example of such a unit and consists of five original connected SP's. We also illustrate the larger RG units employed in our investigations in Figure 4.2 (b). Recall that for any chosen RG unit we must first find the fixed point distribution, $P_c(t)$. In order to do so, in practice, the RG is initialised with some starting distribution (e.g. uniform or Gaussian) of transmission coefficients, $P_0(t)$. From $P_0(t)$, the t_i, $i = 1, .., 5$, are obtained and substituted into the RG transformation. The phases, ϕ_j, $j = 1, .., 4$,

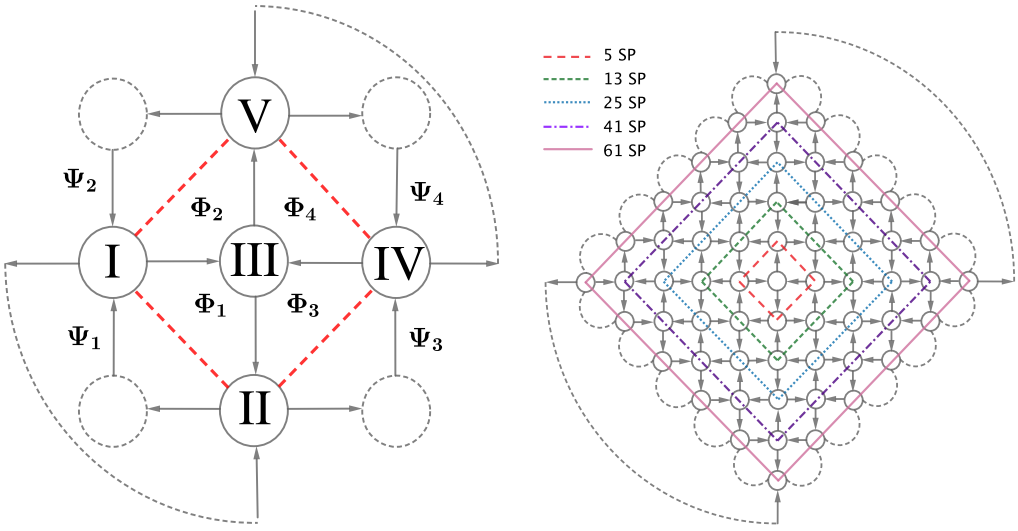

Figure 4.2: (Left) The familiar RG unit from Figure 2.7 with the dashed red lines used as an extra simplified indication of which nodes are left open. (Right) The five main RG cells investigated are represented in this diagram with the saddle point structure of each cell enclosed by its corresponding coloured line analogous to the example on the (Left) diagram.

are also selected randomly from a uniform distribution with range, $[0, 2\pi)$.

In this way, a large number of super transmission coefficients, t', are generated, using the equivalent of Eq. (2.19) for the respective super-cell structure. In practice, one decreass statistical fluctuations of the resulting histogram, $P_1(t)$, by smoothing using a Savitzky-Golay filter, [75]. At the next step the procedure is repeated using $P_1(t)$ as the initial distribution, and so on until convergence of the iteration process is close. I.e. when the mean-square deviation, $R = \int dt[P_n(t) - P_{n-1}(t)]^2$, of the distribution $P_n(t)$ and its predecessor deviate by less than a chosen tolerance which varies with RG structure due to numerical instabilities. Since the transmission and reflection coefficients, t_i and r_i, respectively, are related to the SP heights, z_i,

$$t = \left(\frac{1}{1+e^{z}}\right)^{\frac{1}{2}} \quad , \quad r = \left(\frac{1}{1+e^{-z}}\right)^{\frac{1}{2}} \quad , \tag{4.10}$$

as we previously discussed, we reformulate $P(t)$ as a distribution with respect to z, which we call $Q(z)$. However, the range of z is all $\mathbb{R}$, hence we must use cutoff heights, when doing the numerics to avoid numerical errors caused by the computation of our super transmission coefficients, $t' = t'(t_i : i = 1, .., 5)$, for very small and large t_i. We select the same cut-offs as Gruzberg *et al.* in [30] to maintain consistency and tested the robustness of our critical exponents to varying said cut-offs. Specifically, we worked with $t_i > \epsilon = 10^{-6} \Rightarrow z_i > -35$ and found the robustness claimed in Ref. [30] for $\epsilon \in [10^{-5}, 10^{-7}]$, as the same issue occurs in the TM method by inspection of the matrices in the previous section. Once ϵ is taken outside this range in either direction numerical errors became prevalent which express themselves as an over abundance of t' generated near the cut-off.

In finding a convergent fixed point distribution (see Figure 4.3), $Q_f(z)$, we employ the procedure discussed in Section 2.4, some of which are plotted in Figure 4.3.

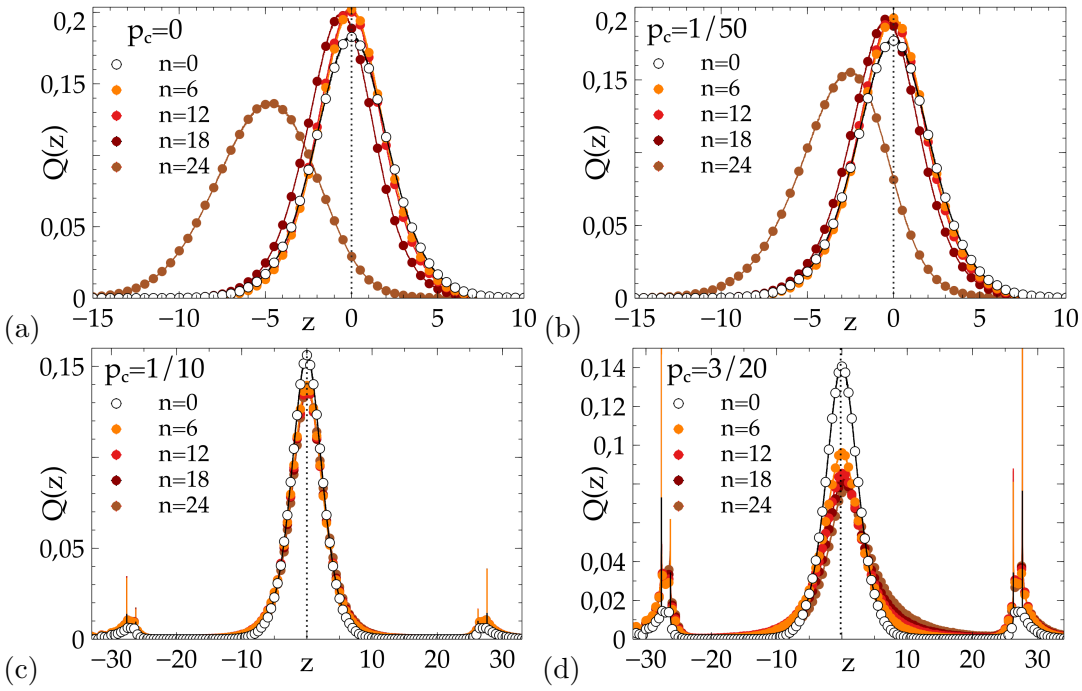

Figure 4.3: The effect on the initial distribution, $Q_0(z)$, (empty circle) once it goes through its RG steps for 5 SP, it is numbered by n with $n = 6, 12, 18, 24$. The four plots show the difference in the FP distributions with respect to various amounts of GD. The vertical dashed line indicates the average of the FP distribution, $Q_f(z)$, ($n = 1$ in all cases studied here). The distribution remains nearly fixed in these cases up until $n = 12$ where it begins to shift.

The working formula for the critical exponent we will be employing is the one derived in Section 2.4,

$$\nu = \frac{n \log s}{\log \frac{z_{\max,n}}{z_0}}, \tag{4.11}$$

As we have previously shown, $z_{max,n}$ depends linearly on z_0, which is illustrated on the RHS of Figure 4.4 for a number of RG steps, n. The leftmost $Q(z)$ in each of the distributions plotted in Figure 4.4 is the fixed point distribution of the respective saddle point structure shifted by $z_0 = 0.1$. The maxima of the distributions, $z_{max,n}$, result in the vertical line of points illustrated by the larger data points in each of the linear plots.

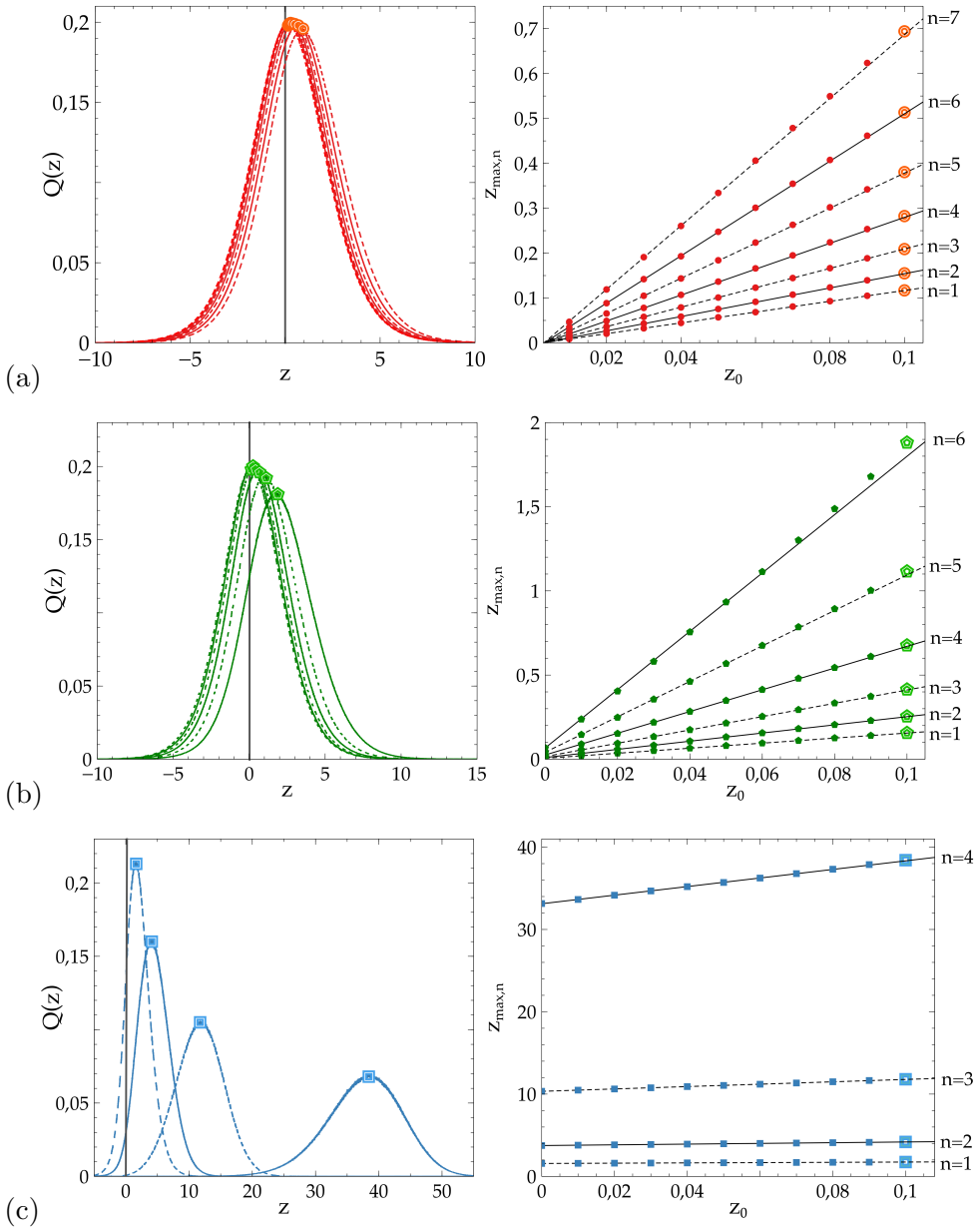

Figure 4.4: The distributions plotted on the left side are of $Q_f(z)$ shifted by $z_0 = 0.1$ ran through a certain number of RG steps, n, for the 5, 13 and 25 SP RG cells which are shown in figures (a), (b) and (c), respectively. The plots on the right side provide ν through the dependence of the $z_{\mathrm{max,n}}$ of $Q_n(z)$ on a small initial shift z_0. Each gradient line fit indicates an RG step for a particular value of z_0, following the example provided by the plots on the left.

If one inspects the linear fits on the right handed plots of Figure 4.4, ν is determined by the dependence of the $z_{\mathrm{max,n}}$ of $Q_n(z)$ on a small initial shift z_0. Each gradient line fit indicates an RG step for a particular value of z_0, following the example on each main plot. The dashed and solid lines are employed for readability. The dashed inset lines map to the dashed (or faded in the case of 61 SP) distributions in the main plot.

The critical coefficient plot is found from the gradients of $z_{\mathrm{max,n}}(z_0)$, since Eq. (4.11) can be reformulated to the following,

$$\nu = \frac{n}{\ln_s \frac{dz_{\mathrm{max,n}}}{dz_0}}. \tag{4.12}$$

The value obtained in this work from the converging slope above for the aforementioned five SP structure example coincides well with the experimentally discovered value. We note that it is clear that the distributions shift further after each RG step for larger super-cells. It is fortunate that this is the case since ν should remain $\mathcal{O}(1)$ for us to consider our model to be accurate and map to other studies of the CC network as well as experiment. The scale factor, s, maintains this balance when one increases with the number of SP's per RG unit, s increases and if the shift size did not increase appropriately as well then the ν would be wildly different for different super SP's even though they maintain the same structure, which would not make physical sense.

On the other hand, a more notable point can be critiqued in the plots of larger SP structures such as 25 and 41 SP supercells (see Figures 4.4 (c) and (d)). It is clear from the first data points in the inset plots linear fits that they shift quickly away from $z_{max,n} = 0$ which should not be the case as these are the FP distributions and they should only shift away from zero at large n; otherwise these distributions cannot be considered fixed. This means that these larger SP structures are not as reliable in the output of their values of the critical exponent as they do

not fulfil the requirements of the RSRG approach. Of course one may follow with the question of why invest the computational effort to study said structures, the answer is simple, when we employ GD in our modified CC network, this has the effect of reducing the shift after every RG step - the larger the GD the smaller the shift (and the more fixed the initial distribution). Thus, it was vital for us to check how strongly the shift is affected, and thus the critical exponent varied, even for the most rapidly shifting super SP.

We studied nine different saddle point structures, the main five of interest, however, are shown in Figure 4.2 (b). In all the cases we studied, as is always the case, no Coulomb interaction between electrons is taken into account; hence it may not be describing the physics entirely.

Chapter 5

Results and Discussion

The original RSRG result by Cain and Römer in Ref. [13] was based on the standard CC network and hence did not involve the open-closed nodes modification. Moreover, as we mentioned earlier, they focused their study on 4 and 5 SP RG units and found that 5 RG units produced results closest to ν_{exp}. This lacked a systematic study of various RG cell structures as well as the GD modification we employed here.

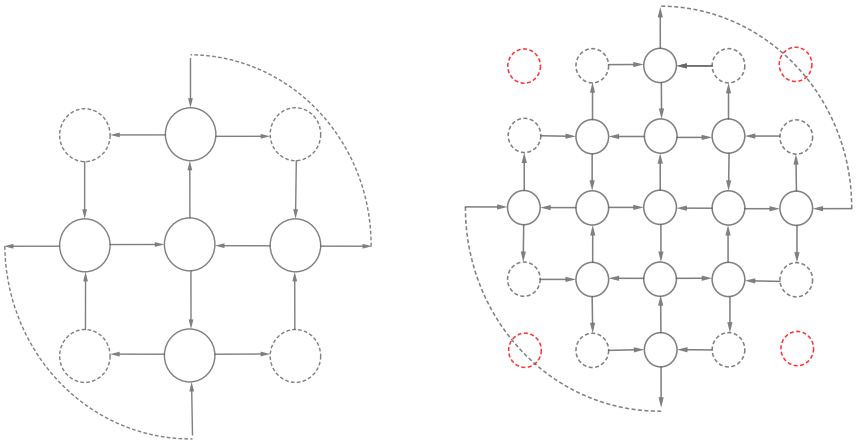

Figure 5.1: We compare 5 SP and 13 SP supercells, (Left) and (Right), respectively, for the difference in the number of active and passive open (dashed) and closed (red) nodes in each cell structure studied.

It is well known that the RSRG approach applied to asymmetric unit cell structures is unreliable, since the input and output symmetry is necessary [74]. An output symmetric cell contains an equal probability for transmission or reflection and hence a symmetric $P(t^2)$ distribution. Input symmetry is necessary since the cell must hold its self-similarity during renormalisation which biases the distribution towards a transmission coefficient.

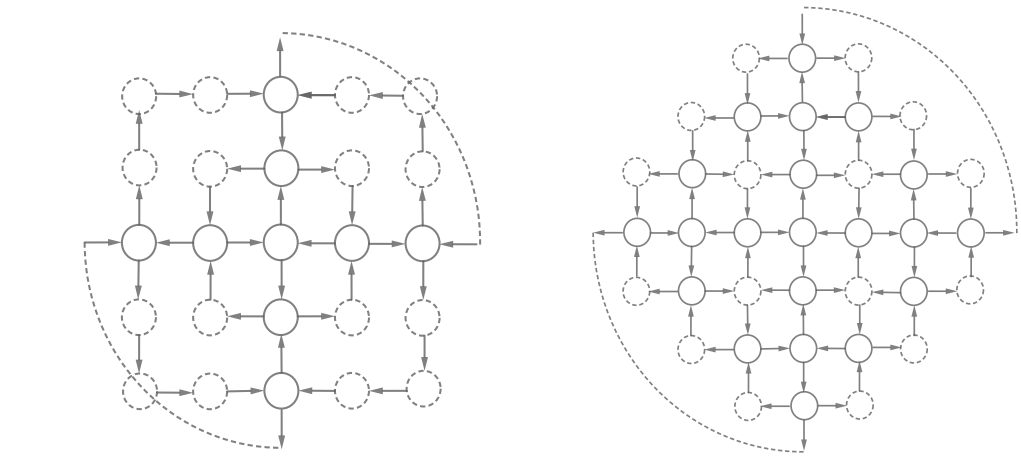

(a) (b)

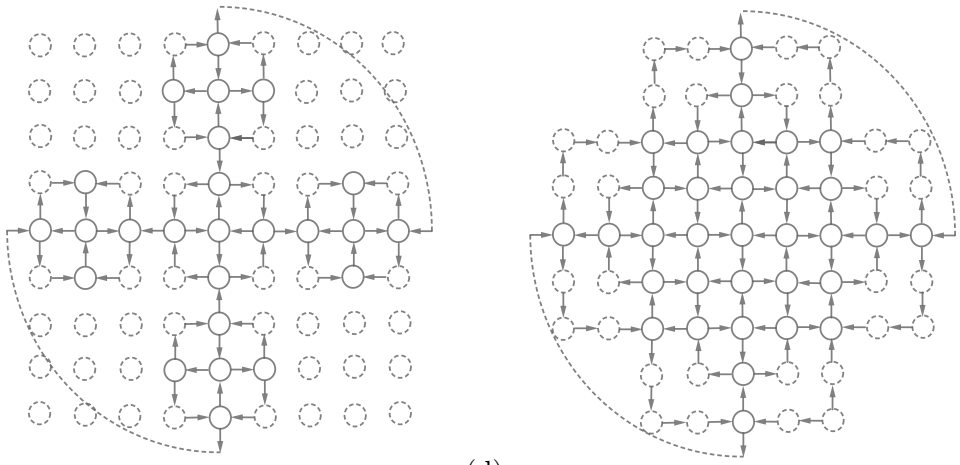

(c) (d)

Figure 5.2: Diagrams of the alternative RG cells studied, included in table5.1. (a), (b), (c) and (d) are diagrammatic representations of the 9, 21, 25(alt.) and 33 SP structures, respectively.

The RG units ability to accurately predict the critical exponent depends on four major properties: significant cell boundary representation, high density of SP's in the same configuration as the CC model, the symmetry of the inputs and outputs and the density of SP's within the cell. The differences between RG cell structures at the SP level need to be outlined to be able to produce deductions based on the structural variants. For example, in Figure 5.1, one can compare the 5 SP structure with the 13 SP structure. The full circles represent active nodes in the square lattice, the dashed circles represent open nodes, and the red circles represent nodes that are left out (effectively closed) from the supercells at each RG step. In our work, we focused on five supercells which satisfied the symmetry requirements, with 5, 13, 25, 41 and 61 SP's and a corresponding scale factor, s, of 2, 4, 6, 8 and 10, respectively (see Figure 4.2 (b)). These were decidedly the most reliable structures to consider since they have the maximum ratio of 'active' to 'passive' nodes with respect to their size as, quantified by the scale factor, s, as well as being maximally symmetric. We also included our results for less reliable supercells (illustrated in Figure 5.2) of the same size for comparison.

5.1 Hypotheses and Statistical Analysis

Although recent work was solved entirely numerically [31, 73, 79], we reduced statistical errors when possible (for the 5 and 13 SP structures) by mimicking the semi-analytical method in Ref. [13]. I.e. we employ the analytic expression for the super transmission coefficient rather than numerically solving the set of equations the coefficient arises from, see Eq. 2.19 for the 5 SP case and although the expression for the 13 SP case is too large to present here it is found analogously to the 5 SP case by solving the system of linear equations. To maximise precision, we generate up to 10^{11} transmission coefficients, N, to obtain our exponents in each case. We also compared our exponents produced with exponents obtained with smaller

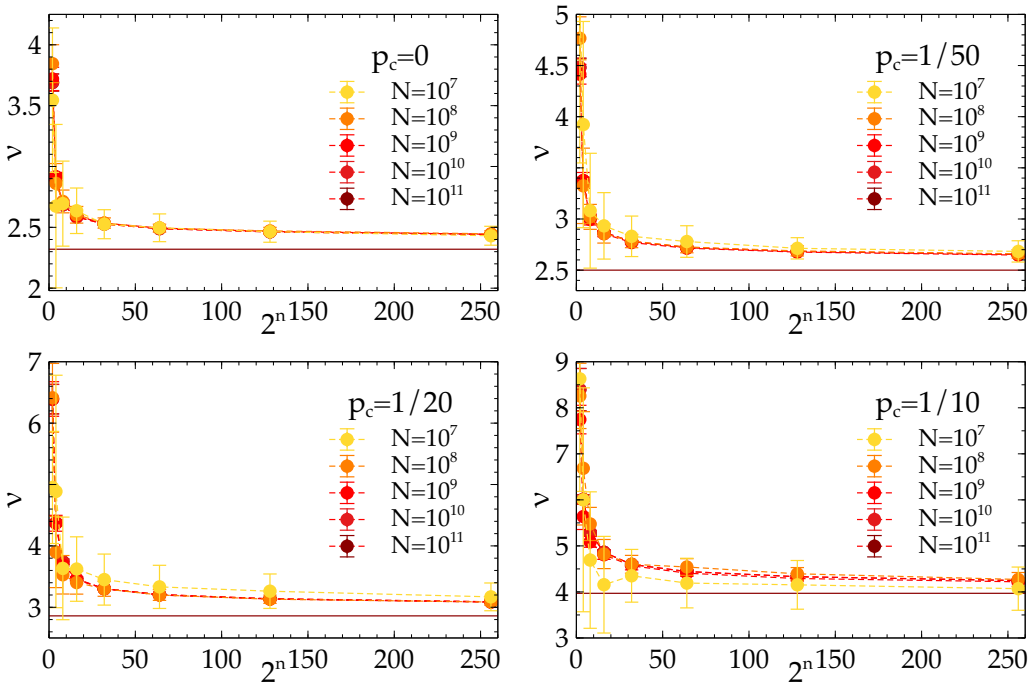

Figure 5.3: The critical exponents of the 5 SP cell, for the values of p_c investigated, with respect to s^n such that n is the number of RG steps and $s = 2$. The horizontal lines indicate our quoted critical exponents in Table 5.1 post-fitting for large n.

$N = 10^{7,9}$. It is clear from Figure 5.3 that little accuracy improvement is obtained when increasing the number TC's in obtaining the critical exponent for $p_{0,1} = 0$; however, the results differ more significantly when $p_{0,1} > 0$ and thus it is more valuable to consider large N as we have done. In each plot of Figure 5.3 one can see that increasing the number of transmission coefficients, N, used in the calculation of ν does little to improve accuracy for lower values of p_c, shifting them down by $\mathcal{O}(10^{-4})$ (see figures (a) and (b)). The shifts, and thus improvements in accuracy, become relevant in this, as well as other RG structures from $p_c = 1/20$ (see figures (c) and (d)) onwards.

We will now discuss our results when maintaining the symmetry of statistical isotropy as well as the results when one breaks this symmetry. In both cases, we obtain a set of critical exponents for different RG structures. Before showing the

results, we will tie up any statistical loose ends and explain how the results are more accurate than previously obtained results in the RSRG approach to attaining the critical exponents. Firstly, as we previously mentioned, the number of transmission coefficients used to calculate the critical exponents is two orders of magnitude larger than previous studies. Secondly, in previous work, the authors took the critical exponent of the last RG step, n, generated to be their quoted critical exponent. Although this is a reasonable estimate, it is by no means optimal since the true exponent lies in the large n limit by definition of the RSRG approach [8]. To remain true to this, we employed a weighted fitting procedure to the critical exponents we generated at each step. The function, $\nu(n) = \nu\left(n, \frac{dz_{\mathrm{max,n}}}{dz_0}\right)$, needs to be found in the large n limit, at which point ν converges to a constant value. Thus by rearranging Eq. (4.11),

$$\log \frac{dz_{\mathrm{max,n}}}{dz_0} = \frac{\log s}{\nu} n + \delta, \tag{5.1}$$

where we added a small constant δ as a secondary fit parameter to improve the gradient fit (this is necessary due to the limited number of data points, since the maximum n we have is $n = 8$). We can ignore δ once we take the large n limit. Let us now define $\log s/\nu = \alpha$, where α is a constant and $\frac{dz_{\mathrm{max,n}}}{dz_0} = A(n)$ in the limit. Thus, we commit to a linear regression, two parameter, (α, δ), fit to accomplish in finding the final value of the critical exponent,

$$\nu = \frac{n \log s}{\log A(n)} = \frac{n \log s}{\alpha n + \delta}, \tag{5.2}$$

We display the linear fits along with the fits of the corresponding Eq. (5.2) in Figure 5.4. As is clear from the linear fits of Figure 5.4, the values for δ are indeed small, of $\mathcal{O}(10^{-2})$ or less, because $\log A(n)$ exhibits its linear nature early on, which is ideal. Thus, once α is obtained along with its confidence interval, the critical exponent is

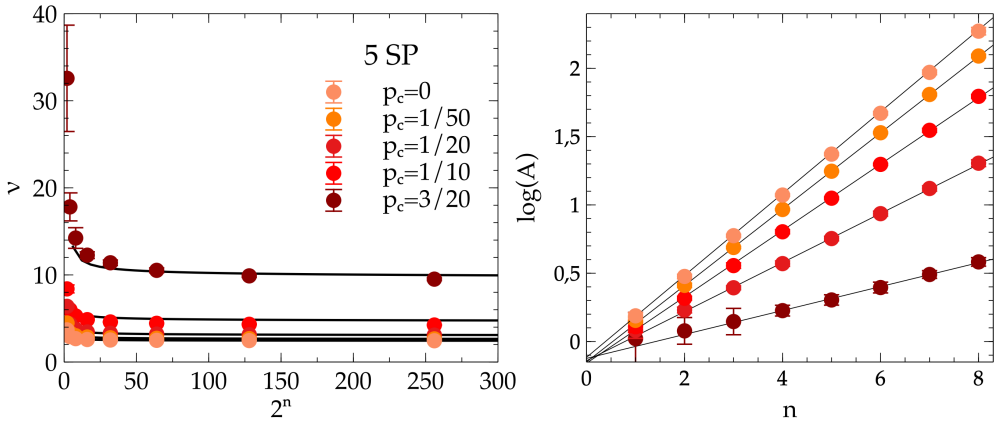

Figure 5.4: (Left) The plots of ν versus n generated from $N = 10^{11}$ transmission coefficients for various values of p_c. The number of RG steps along with their fits are obtained from the gradients of the inset plot. (Right) the lines one obtains from the gradients, $A(n)$, for various p_c used in the final calculations of ν.

easily found by taking the large n limit of Eq. (5.2),

$$\nu_{cc} = \frac{\ln s}{\alpha} \tag{5.3}$$

It is also useful to note that since we reduced the problem to a linear fit, the measures of goodness of fit generated illustrated excellent agreement with the data, for instance, the adjusted R^2 [14] was consistently found to be 98% or higher - for comparison a value of 90% or higher means that the fit explains all the variability of the data around its mean. On the other hand, the precision of our exponents, described by the 95% confidence intervals presented in Table 5.1, starts to get challenged due to numerical errors at larger values of GD as well as for RG cell structures which take into account more SP's as we will see in the upcoming sections.

Lastly, we should make a note on the skewness of the distributions, $Q(z)$, generated to find $z_{max,n}$, which is a well-known measure of the true randomness of a given distribution [47]. The skewness is plotted in Figure 5.5 for the main RG structures studied. It is clear from the plots that the 5SP structure exhibits the smallest shift in skewness, γ, as z_0 and n increase. Moreover, it maintains a low

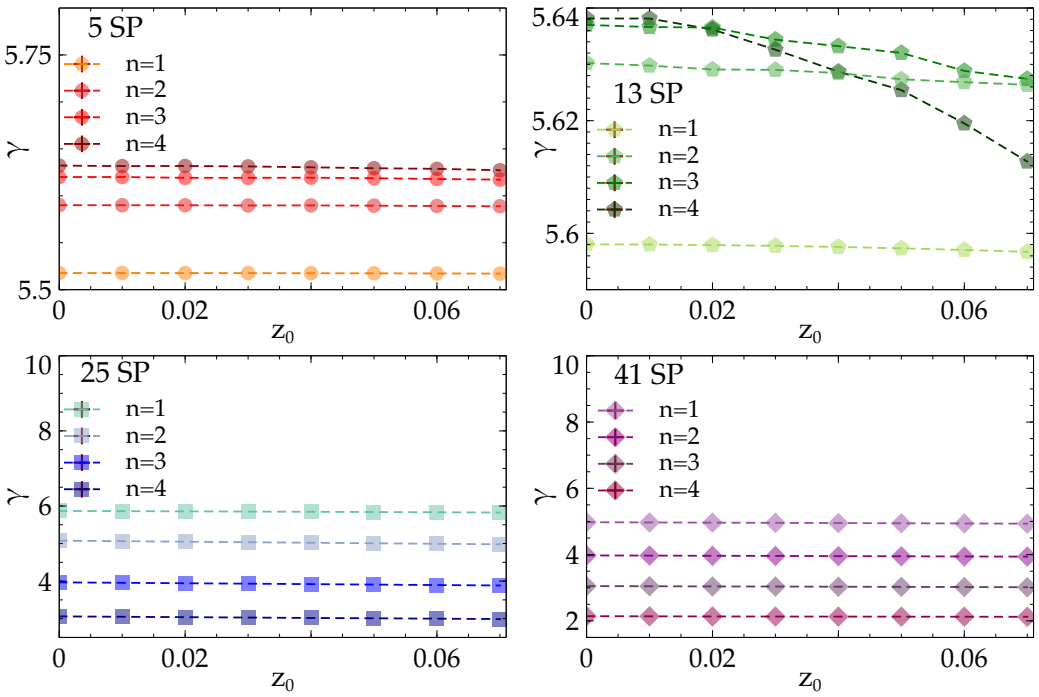

Figure 5.5: Plots of the skewness, γ, of the main RG structures for varying SP height shift, z_0, and RG steps, n.

value of γ throughout which decreases as n increases. As for the larger structures, γ is initially large but shift downwards significantly as n increases. However, at larger values of n where the skewness is small, numerical instability we discussed previously starts to come into play due to the higher proportion of transmission coefficients generated near cut-off; thus the 5 SP structure remains the most reliable in its exhibition of randomness.

5.2 Unbroken Statistical Isotropy

We begin by considering the case when $p_0 = p_1 = p_c$ from zero upwards. We find that past $p_c = 3/20$, the precision of our result begins to become compromised in some cell structures due to the decrease of data points near the maximum of the $Q(z)$ distribution. A clear trend is visible which remains valid in all cell structures we examined, there is a clear upwards shift of the critical exponent, ν, as p_c increased.

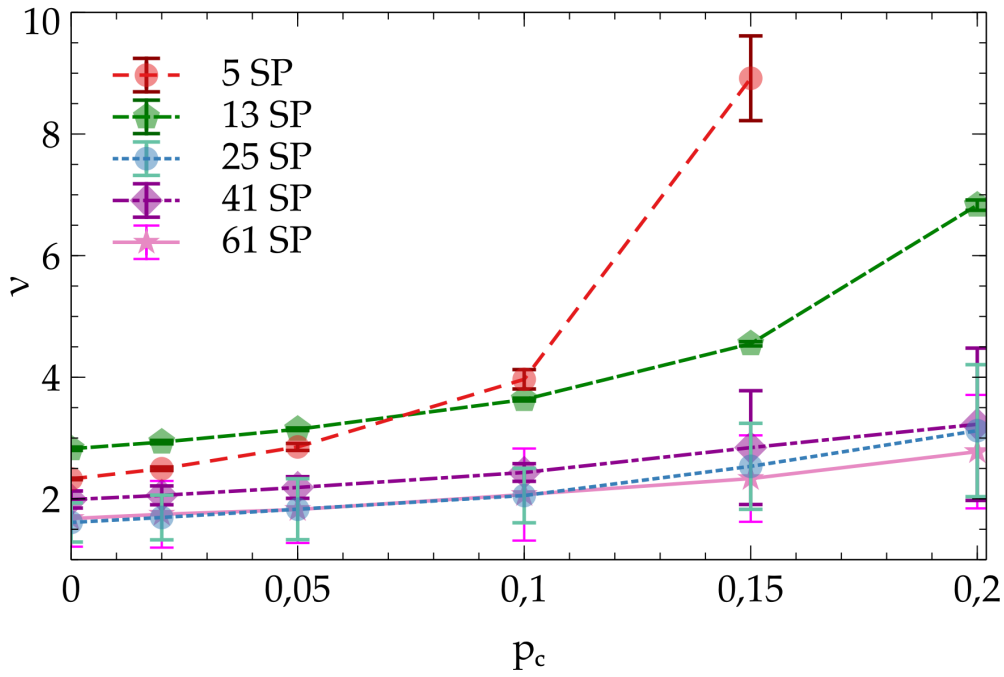

Figure 5.6: Critical exponents obtained for RSRG method applied to the modified CC network with the five main RG cells. It is clear that for each RG cell modelled the curves have a positive divergence.

The results we obtained for ν with respect to s^n, where s is the scale factor and n is the number of RG steps, are plotted in Figure 5.6. By inspection of Figure 5.6, it is clear that for each RG cell structure, the critical exponents do not overlap. Thus, we found a line of critical exponents as a function of p_c for each RG super cell studied. The final numerical values of the critical exponents obtained are also present in Table 5.1, where we include more modified critical exponents, $\nu_{\text{cc,mod}}$, for the less reliable RG cell structures (exhibited in Figure 5.2) as well as higher values of p_c, in the cases where numerically induced uncertainties were small. If one reads across Table 5.1, there is a clear trend towards lower values (modulo fluctuations which occur in classical BPT as well) of the critical exponent. Hence, one can conclude that increasing the number of SP's per RG cell decreases the effective critical exponent. Another observation one may make from looking down Table 5.1 is that the larger the RG cell, when GD is increased, the change in ν, $\Delta\nu$, decreases.

Thus, it is clear from this monotonic decrease that the larger the number of SP's in the primary structures we are investigating, the more robust the critical exponent is to GD. The reasoning behind this will be analysed and further discussed in the upcoming section.

5.3 Broken Statistical Isotropy

We now consider the statistically anisotropic case when $p_0 \neq p_1$, and thus the number of active and passive nodes caused by GD are not equal on average in this case. We focused on the bimodal result in which $p_0 = 0$, $p_1 = 1$ and vice versa, this was done to extremise the asymmetry. In each of these cases, as in the isotropic case, we found that past a certain amount of GD, specifically, $p_{0,1} = 1/5$, the precision of our result began to become compromised due to numerical instabilities in the cell structures studied. Once more, we maintained the same cut-off value of $\epsilon = 10^{-6}$ and found the same robustness in the values for the critical exponent were exhibited as in the isotropic case.

The values for the critical exponents we obtained for four of the main saddle point structures are plotted in Figure 5.7. The critical exponents for the 61 SP structure were left out due to their unreliability caused by the substantial effects of numerical errors on larger RG cells in the anisotropic cases. By inspection of the plots in Figure 5.7, the trend is less obvious, and the numerical errors are more prevalent for larger RG structures. As we mentioned in the previous section, one can view the full set of exponents as they are presented in Table 5.1. One can see from Table 5.1 that the trend of the critical exponents in the case where $p_1 = 0$ and $p_0 > 0$ (increasing the number of passive closed nodes per RG unit) is decreasing as p_0 unanimously across the different SP structures. Furthermore, the robustness seen in the isotropic case across larger structures is conserved. On the other hand, in the converse case when one solely increases the number of open nodes the critical

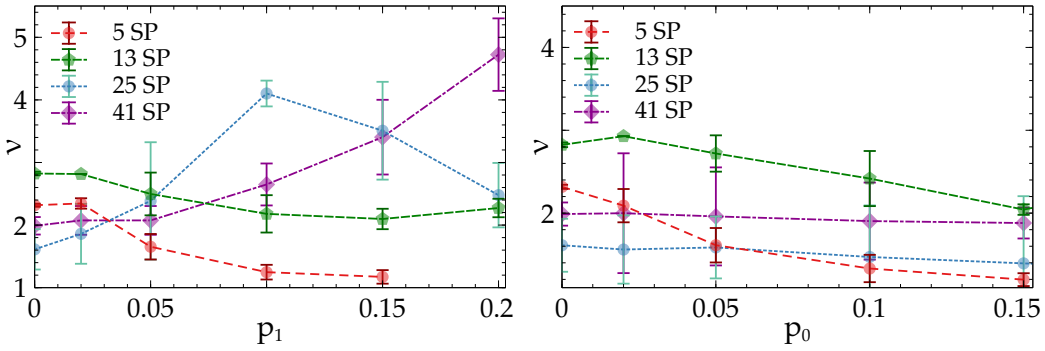

Figure 5.7: Critical exponents obtained for RSRG method applied to the anisotropic modified CC network with four of the main RG cells studied. (Left) illustrates the case $(p_1 > 0, p_0 = 0)$ and (Right) the converse case where $(p_0 > 0, p_1 = 0)$.

exponents no longer vary monotonically in the mid-sized structures. In particular, with regards to the 13 SP structure, one can see that the critical exponent appears to be decreasing from the value at $p_0 = p_1 = 0$, except for the upwards shift near $p_1 = 3/20$. Similarly, with the 25 SP structure, the critical exponent climbs up until around $p_1 = 1/10$ and then starts to decrease. As for the 5 and 41 SP structures, the exponents are monotonically decreasing and increasing, respectively.

	5 SP	13 SP	25 SP	41 SP	61 SP		9 SP	21 SP	25 SP (alt.)	33 SP
Active	5	13	25	41	61		9	21	25	33
Passive Open	4	8	12	16	20		4	16	24	32
Passive Closed	0	4	12	24	40		12	12	32	16
$p_c = 0$	2.33(1)	2.82(3)	1.61(32)	1.99(14)	1.68(46)		4.41(2)	5.49(5)	6.05(5)	3.13(19)
$p_c = 1/50$	2.50(3)	2.93(3)	1.69(37)	2.06(16)	1.75(55)		4.69(4)	5.74(5)	6.39(3)	3.58(78)
$p_c = 1/20$	2.85(6)	3.14(2)	1.83(50)	2.19(18)	1.82(55)		5.23(9)	6.37(10)	7.09(29)	3.17(38)
$p_c = 1/10$	3.97(16)	3.63(2)	2.05(45)	2.43(15)	2.07(76)		6.73(22)	6.74(60)	8.60(13)	3.66(45)
$p_c = 3/20$	8.92(70)	4.55(4)	2.53(71)	2.84(94)	2.33(71)		11.2(7)	11.1(9)	11.8(2)	3.59(50)
$p_c = 1/5$		6.83(8)	3.12(1.09)	3.23(1.25)	2.78(93)				22.8(1.4)	5.65(1.39)
$p_c = 1/3$					23.5(7.1)					
$p_0 = 1/50, p_1 = 0$	2.09(20)	2.929(4)	1.56(41)	1.99(72)						
$p_0 = 1/20, p_1 = 0$	1.61(21)	2.72(22)	1.59(37)	1.96(59)						
$p_0 = 1/10, p_1 = 0$	1.33(16)	2.42(33)	1.47(62)	1.90(47)						
$p_0 = 3/20, p_1 = 0$	1.20(7)	2.04(6)	1.39(81)	1.88(19)						
$p_1 = 1/50, p_0 = 0$	2.35(08)	2.815(1)	1.86(48)	2.07(23)						
$p_1 = 1/50, p_0 = 0$	1.65(20)	2.50(34)	2.39(93)	2.23(27)						
$p_1 = 1/10, p_0 = 0$	1.25(12)	2.18(30)	4.10(21)	2.65(34)						
$p_1 = 3/20, p_0 = 0$	1.17(11)	2.10(16)	3.51(78)	3.40(60)						
$p_1 = 1/5, p_0 = 0$		2.27(15)	2.48(51)	4.72(58)						

Table 5.1: Statically isotropic and anisotropic critical exponents for the RG cells studied with indications of their node structure.

5.4 Discussion

For the discussion of our results we will use Table 5.1 as a reference, which displays the number of active and passive nodes in the various RG cells we studied. It is clear from the table that as was previously stated, solely the main five RG structures have more active than passive nodes (one more to be exact), the alternative structures with more passive to active are shown in Figure 5.2. It is clear, by inspection, that the five SP structure has the largest ratio of active to passive nodes. Moreover, this ratio tends closer to one as the cells get larger; it is thus useful to study the larger structures in the modified case. The GD modification involves imposing a change from active to passive (equal number of open and closed in the isotropic case and conversely in the anisotropic case).

Our results raise some intriguing questions; for example, it would seem to be the case that the GD employed is highly dependent on the initial SP structure, in the CC model it is always a regular square lattice - which is well represented in the TM method. However, in the RSRG method the SP cells approximate a regular lattice to zeroth order (with a scale factor), the structure is fundamentally different. This is clear by inspection of the tunability of the critical exponents as the GD is varied for a particular base SP structure.

Chapter 6

Summary and Outlook

It is important to investigate further symmetry classes to gain a foothold on the utility of our results. One can construct network models for all ten symmetry classes of disordered systems, which can be found in Refs. [71]. In particular, superconductors with broken time-reversal invariance in two dimensions can exhibit QH transitions where the spin (SQH - symmetry class C) [76] and thermal (TQH - symmetry class D) [49] conductivities jump in quantised units. The ideas developed can surely be extended to particular network models of these and other elusive transitions. Besides, both the SQH and TQH are more straightforward in many ways to study than the IQH since a large number of their properties are determinable by mapping to well-understood classical models.

For example, the regular network in symmetry class C was linked to classical bond percolation on a simple square lattice [48, 66]. Many exact results are known for classical percolation; therefore, the mapping has led to a range of exact critical properties at the SQH transition. Moreover, said mapping was extended to network models in class C for arbitrary graphs [85]. The graphs relevant for our study are shown in Figure 3.1. For a given RN we draw the dual bipartite graph with dots on the shaded faces and crosses on the blank faces of the original RN. The dual graph forms a random quadrangulation of the plane. We now dissect all quadrangles by

diagonals connecting the dots and remove the crosses and all edges connected to them. This results in a lattice (Figure 3.1, right) on which the classical bond percolation should be considered. Critical bond percolation on random quadrangulations (or their dual network - Figure 3.1, right) was considered in Ref. [46], and it was shown that the KPZ relations are valid in this case. We believe that the SQH transition on RNs lies in the same universality class and that KPZ can be applied to all critical exponents obtained in Refs. [25, 6, 66, 48]. This includes, in particular, the dimension of the two-leg operator that determines the localisation length exponent, ν, as well as a few MF exponents.

The TQH transition can also be described and simulated by a network model [77, 61]. Its effective field theory (without GD) is given by the Majorana fermions with random mass, the same theory that describes the critical Ising model with a weak bond disorder [49, 31]. The random mass is a marginally irrelevant perturbation, and critical exponents at the transition are given by their Ising model values. When the model is coupled to 2D QG, we still should consider the quenched situation, and the critical exponents should be modified according to the KPZ relations, see [4] and references therein. The geometric disorder that we simulated in our work by a modified CC model can be viewed as randomness in the heights, V, of the saddle points in the disorder potential. It is well known that (at electron energy, $\epsilon_e = 0$) $t^2 = (1 + e^V)^1$ [27]. The t we have chosen in our modified CC model is described by the tri-modal distribution,

$$P(V) = p_0\delta(V - 2\log\epsilon) + p_c\delta(V) + p_1\delta(V + 2\log\epsilon) \tag{6.1}$$

Previous studies of random V [93, 94] focused instead on the uniform distribution (or regular CC network) in the interval $V \in [W, W]$ or the bi-modal distribution,

$$P(V) = [\delta(V - W) + \delta(V + W)]/2. \tag{6.2}$$

However, no choice of W mimics our type of randomness when $p_c > 0$. On the other hand, for $p_c = 0$, our distribution becomes bi-modal, and describes a classical 2D percolation model with $\nu = 4/3$. The other extreme, $p_c = 1$, gives the regular CC model.

Since previous work by Gruzberg *et al.* only simulated the point $p_c = 1/3$ with poor statistics, they could not distinguish between the following three possibilities: a novel fixed point at a finite p_c, a crossover from percolation to CC criticality or a line of fixed points. In our work, we studied a range of values of $p_c < 1/3$ with the RSRG approach at very high precision and determined a line of fixed points exist independent of the RG unit being employed, as long as said unit captures the physics of the underlying original network faithfully. It is crucial now to start to simulate RN's in classes C and D and try to solve the classical percolation problem on relevant graphs using matrix models techniques. Moreover, one must further study the problem of Dirac fermions in an Abelian random gauge potential coupled to 2D QG, to determine the multifractality spectrum of the wave functions in order to test the validity of applying the KPZ relation to each case.

In summary, the existence of a new type of geometric disorder was proposed and, we tested in a novel and broad fashion not previously achieved by the original authors. We have determined that GD allows one to tune critical exponents depending on how it is applied independently of the RG unit cell chosen if one employs the RSRG method. We have thus determined that GD changes the universality class of the model it is applied to - in our case the CC model and our numerical results support this claim. We have also reiterated the possibility that 2D QG coupled to matter fields provide the proper framework for a field-theoretic description of this type of disorder. These ideas can be further applied to other 2D Anderson-type transitions, and it would be intriguing to see how they alter the playing field.

Bibliography

[1] M. Amado, A. V. Malyshev, A. Sedrakyan, and F. Domínguez-Adame. Numerical Study of the Localization Length Critical Index in a Network Model of Plateau-Plateau Transitions in the Quantum Hall Effect. *Physical Review Letters*, 107(6):066402, 8 2011. ISSN 0031-9007. doi: 10.1103/PhysRevLett.107.066402. URL https://link.aps.org/doi/10.1103/PhysRevLett.107.066402.

[2] J. Ambjørn, K. N. Anagnostopoulos, U. Magnea, and G. Thorleifsson. Geometrical interpretation of the Knizhnik-Polyakov-Zamolodchikov exponents. *Physics Letters, Section B: Nuclear, Elementary Particle and High-Energy Physics*, 388(4):713–719, 1996. ISSN 03702693. doi: 10.1016/S0370-2693(96)01222-1.

[3] P. W. Anderson. Absence of Diffusion in Certain Random Lattices. *Physical Review*, 109(5):1492–1505, 3 1958. ISSN 0031-899X. doi: 10.1103/PhysRev.109.1492. URL https://link.aps.org/doi/10.1103/PhysRev.109.1492.

[4] E. J. Beamond, John Cardy, and J. T. Chalker. Quantum and classical localization, the spin quantum Hall effect, and generalizations. *Physical Review B*, 65(21):214301, 5 2002. ISSN 0163-1829. doi: 10.1103/PhysRevB.65.214301. URL https://link.aps.org/doi/10.1103/PhysRevB.65.214301.

[5] C. W. J. Beenakker. Random-Matrix Theory of Quantum Transport. 12 1996. doi: 10.1103/RevModPhys.69.731. URL http://arxiv.org/abs/cond-mat/9612179http://dx.doi.org/10.1103/RevModPhys.69.731.

[6] A.A. Belavin, A.M. Polyakov, and A.B. Zamolodchikov. Infinite conformal symmetry in two-dimensional quantum field theory. *Nuclear Physics B*, 241(2):333–380, 7 1984. ISSN 05503213. doi: 10.1016/0550-3213(84)90052-X. URL http://linkinghub.elsevier.com/retrieve/pii/055032138490052X.

[7] E. Bettelheim, I. A. Gruzberg, and A. W. W. Ludwig. Quantum Hall transitions: An exact theory based on conformal restriction. *Physical Review B*, 86(16):165324, 10 2012. ISSN 1098-0121. doi: 10.1103/PhysRevB.86.165324. URL https://link.aps.org/doi/10.1103/PhysRevB.86.165324.

[8] JJ Binney, NJ Dowrick, AJ Fisher, and MEJ Newman. *The theory of critical phenomena: an introduction to the renormalization group*. 1992. URL https://sci-hub.tw/https://books.google.com/books?hl=en&lr=&id=BCOQDwAAQBAJ&oi=fnd&pg=PP1&dq=real+space+renormalization+group+theory&ots=wV5qEIn9Fe&sig=hIRymOUoItUKLkyeoV-tfNYOQu0.

[9] S. T. Bramwell, P. C. W. Holdsworth, and J.-F. Pinton. Universality of rare fluctuations in turbulence and critical phenomena. *Nature*, 396(6711):552–554, 12 1998. ISSN 0028-0836. doi: 10.1038/25083. URL http://www.nature.com/articles/25083.

[10] I.S. Burmistrov, S. Bera, F. Evers, I.V. Gornyi, and A.D. Mirlin. Wave function multifractality and dephasing at metalinsulator and quantum Hall transitions. *Annals of Physics*, 326(6):1457–1478, 6 2011. ISSN 0003-4916. doi: 10.1016/J.AOP.2011.01.005. URL https://www.sciencedirect.com/science/article/pii/S0003491611000273.

[11] Tsallis C and Schwachheim G. Real-space renormalisation group: application to site percolation in square lattices. *J. Phys. C: Solid State Phys.*, 12(9), 1979. URL http://0-iopscience.iop.org.pugwash.lib.warwick.ac.uk/article/10.1088/0022-3719/12/1/014/pdf.

[12] ME Cage, K Klitzing, AM Chang, F Duncan, and M Haldane. *The quantum Hall effect*. 2012. URL https://sci-hub.tw/https://books.google.com/books?hl=en&lr=&id=mxrSBwAAQBAJ&oi=fnd&pg=PR5&dq=integer+quantum+hall+experiment+nobel&ots=4ujtsUI5hV&sig=FKVPNN4Jq-le5he8PRL-TAQlVTs.

[13] P. Cain, M.E. Raikh, and R.A. Römer. Real-space renormalization group approach to the quantum hall transition. *Journal of the Physical Society of Japan*, 72(SUPPL. A), 2003. ISSN 00319015. doi: 10.1143/JPSJ.72.135.

[14] AC Cameron, FAG Windmeijer Journal of econometrics, and undefined 1997. An R-squared measure of goodness of fit for some common nonlinear regression models. *Elsevier*. URL https://sci-hub.tw/https://www.sciencedirect.com/science/article/pii/S0304407696018180.

[15] John Cardy. Conformal Invariance and Percolation. 3 2001. URL http://arxiv.org/abs/math-ph/0103018.

[16] Horacio E. Castillo, Claudio de C. Chamon, Eduardo Fradkin, Paul M. Goldbart, and Christopher Mudry. Exact calculation of multifractal exponents of the critical wave function of Dirac fermions in a random magnetic field. 6 1997. doi: 10.1103/PhysRevB.56.10668. URL http://arxiv.org/abs/cond-mat/9706084http://dx.doi.org/10.1103/PhysRevB.56.10668.

[17] J T Chalker and P D Coddington. Percolation, quantum tunnelling and the integer Hall effect. *Journal of Physics C: Solid State Physics J J. Phys. J. Phys. C: Solid State Phys*, 21(21):2665–2665, 1988. URL http://0-iopscience.iop.org.pugwash.lib.warwick.ac.uk/article/10.1088/0022-3719/21/14/008/pdf.

[18] Kim Christensen. Percolation Theory. Technical report, 2002. URL http://www.cmth.ph.ic.ac.uk/kim/cmth/.

[19] Franois David and Michel Bauer. Another derivation of the geometrical KPZ relations. *Journal of Statistical Mechanics: Theory and Experiment*, 2009(03):P03004, 3 2009. ISSN 1742-5468. doi: 10.1088/1742-5468/2009/03/P03004. URL http://stacks.iop.org/1742-5468/2009/i=03/a=P03004?key=crossref.e42c4842a2342affadad5b4b2651d8d7.

[20] A C N De Magalhiies, C Tsallis, and G Schwachheim. Probability renormalisation group treatment of bond percolation in square, cubic and hypercubic lattices. *Journal of Physics C: Solid State Physics J. Phys. J. Phys. C : Solid St. Phys*, 13(13):321–30, 1980. URL http://0-iopscience.iop.org.pugwash.lib.warwick.ac.uk/article/10.1088/0022-3719/13/3/006/pdf.

[21] Jacques Distler and Hikaru Kawai. Conformal field theory and 2D quantum gravity. *Nuclear Physics B*, 321(2):509–527, 7 1989. ISSN 0550-3213. doi: 10.1016/0550-3213(89)90354-4. URL https://www.sciencedirect.com/science/article/pii/0550321389903544.

[22] J. S. Dowker. Conformal properties of the heat-kernel expansion. Application to the effective Lagrangian. *Physical Review D*, 39(4):1235–1238, 2 1989. ISSN 0556-2821. doi: 10.1103/PhysRevD.39.1235. URL https://link.aps.org/doi/10.1103/PhysRevD.39.1235.

[23] Bertrand Duplantier and Ivan K. Kostov. Geometrical critical phenomena on a random surface of arbitrary genus. *Nuclear Physics B*, 340(2-3):491–541, 8 1990. ISSN 0550-3213. doi: 10.1016/0550-3213(90)90456-N. URL https://www.sciencedirect.com/science/article/pii/055032139090456N.

[24] Bertrand Duplantier and Kyung-Hoon Kwon. Conformal Invariance and Intersections of Random Walks. *Physical Review Letters*, 61(22):2514–2517, 11 1988. ISSN 0031-9007. doi: 10.1103/PhysRevLett.61.2514. URL https://link.aps.org/doi/10.1103/PhysRevLett.61.2514.

[25] F. Evers, A. Mildenberger, and A. D. Mirlin. Multifractality at the Quantum Hall Transition: Beyond the Parabolic Paradigm. *Physical Review Letters*, 101(11):116803, 9 2008. ISSN 0031-9007. doi: 10.1103/PhysRevLett.101.116803. URL https://link.aps.org/doi/10.1103/PhysRevLett.101.116803.

[26] Ferdinand Evers and Alexander D. Mirlin. Anderson transitions. *Reviews of Modern Physics*, 80(4):1355–1417, 10 2008. ISSN 0034-6861. doi: 10.1103/RevModPhys.80.1355. URL https://link.aps.org/doi/10.1103/RevModPhys.80.1355.

[27] H. A. Fertig and B. I. Halperin. Transmission coefficient of an electron through a saddle-point potential in a magnetic field. *Physical Review B*, 36(15):7969–7976, 11 1987. ISSN 0163-1829. doi: 10.1103/PhysRevB.36.7969. URL https://link.aps.org/doi/10.1103/PhysRevB.36.7969.

[28] RP Feynman, ARHQ Mechanics Lecture Notes Phys, and undefined 1979. Path integrals. *Springer*. URL https://sci-hub.tw/http://www.springerlink.com/index/KJ07X7806672G002.pdf.

[29] I. C. Fulga, F. Hassler, A. R. Akhmerov, and C. W. J. Beenakker. Topological quantum number and critical exponent from conductance fluctuations at the quantum Hall plateau transition. *Physical Review B*, 84(24):245447, 12 2011. ISSN 1098-0121. doi: 10.1103/PhysRevB.84.245447. URL https://link.aps.org/doi/10.1103/PhysRevB.84.245447.

[30] I A Gruzberg, A Klümper, W Nuding, and A Sedrakyan. Geometrically disordered network models, quenched quantum gravity, and critical behavior at quantum Hall plateau transitions. *Physical Review B*, 95(12):125414, 3 2017. ISSN 2469-9950. doi: 10.1103/PhysRevB.95.125414. URL https://0-journals-aps-org.pugwash.lib.warwick.ac.uk/prb/pdf/10.1103/PhysRevB.95.125414https://link.aps.org/doi/10.1103/PhysRevB.95.125414.

[31] Ilya A. Gruzberg, Andreas W. W. Ludwig, and N. Read. Exact Exponents for the Spin Quantum Hall Transition. *Physical Review Letters*, 82(22):4524–4527, 5 1999. ISSN 0031-9007. doi: 10.1103/PhysRevLett.82.4524. URL https://link.aps.org/doi/10.1103/PhysRevLett.82.4524.

[32] Thomas Guhr. Supersymmetry in Random Matrix Theory. 5 2010. URL http://arxiv.org/abs/1005.0979.

[33] Yasuhiro Hatsugai. Chern number and edge states in the integer quantum Hall effect. *Physical review letters*, 71(22):3697–3700, 11 1993. ISSN 1079-7114. doi: 10.1103/PhysRevLett.71.3697. URL https://link.aps.org/doi/10.1103/PhysRevLett.71.3697http://www.ncbi.nlm.nih.gov/pubmed/10055049.

[34] Yasuhiro Hatsugai, Xiao-Gang Wen, and Mahito Kohmoto. Disordered Critical Wave functions in Random Bond Models in Two Dimensions – Random Lattice Fermions at $E=0$ without Doubling. 3 1996. doi: 10.1103/PhysRevB.56.1061. URL http://arxiv.org/abs/cond-mat/9603169http://dx.doi.org/10.1103/PhysRevB.56.1061.

[35] C.-M. Ho and J. T. Chalker. Models for the integer quantum Hall effect: The network model, the Dirac equation, and a tight-binding Hamiltonian. *Physical Review B*, 54(12):8708–8713, 9 1996. ISSN 0163-1829. doi: 10.1103/PhysRevB.54.8708. URL https://link.aps.org/doi/10.1103/PhysRevB.54.8708.

[36] B Huckestein. Scaling and Universality in the Integer Quantum Hall Effect. *Europhysics Letters (EPL)*, 20(5):451–456, 11 1992. ISSN 0295-5075. doi: 10.1209/0295-5075/20/5/012. URL http://stacks.iop.org/0295-5075/20/i=5/a=012?key=crossref.5e6585b60af3a60660553412d5bb6452.

[37] Bodo Huckestein. Scaling theory of the integer quantum Hall effect. *Reviews of Modern Physics*, 67(2):357–396, 4 1995. ISSN 0034-6861. doi: 10.1103/RevModPhys.67.357. URL https://link.aps.org/doi/10.1103/RevModPhys.67.357.

[38] Bodo Huckestein and Bernhard Kramer. One-parameter scaling in the lowest Landau band: Precise determination of the critical behavior of the localization length. *Physical Review Letters*, 64(12):1437–1440, 3 1990. ISSN 0031-9007. doi: 10.1103/PhysRevLett.64.1437. URL https://link.aps.org/doi/10.1103/PhysRevLett.64.1437.

[39] Y. Huo and R. N. Bhatt. Current carrying states in the lowest Landau level. *Physical Review Letters*, 68(9):1375–1378, 3 1992. ISSN 0031-9007. doi: 10.1103/PhysRevLett.68.1375. URL https://link.aps.org/doi/10.1103/PhysRevLett.68.1375.

[40] NOBUYUKI ISHIBASHI. THE BOUNDARY AND CROSSCAP STATES IN CONFORMAL FIELD THEORIES. *Modern Physics Letters A*, 04(03):251–264, 2 1989. ISSN 0217-7323. doi: 10.1142/S0217732389000320. URL http://www.worldscientific.com/doi/abs/10.1142/S0217732389000320.

[41] C Itzykson, H Saleur, and Z Jean-bernard. *Conformal invariance and applications to statistical mechanics*. 1998. URL https://sci-hub.tw/https://books.google.com/books?hl=en&lr=&id=xHHFCwAAQBAJ&oi=fnd&pg=PR5&dq=conformal+field+theory+statistical+mechanics&ots=2boEA1yOvz&sig=RsgdSfLYw3FEZbB_irLD-mClbVI.

[42] J. Jacobsen, N. Read, and H. Saleur. Traveling Salesman Problem, Conformal Invariance, and Dense Polymers. *Physical Review Letters*, 93(3):038701, 7 2004. ISSN 0031-9007. doi: 10.1103/PhysRevLett.93.038701. URL https://link.aps.org/doi/10.1103/PhysRevLett.93.038701.

[43] Janke, Johnston, and Weigel. Two-dimensional quantum gravity - a laboratory for fluctuating graphs and quenched connectivity disorder. *Condensed Matter Physics*, 9 (2):263, 2006. ISSN 1607324X. doi: 10.5488/CMP.9.2.263. URL http://www.icmp.lviv.ua/journal/zbirnyk.46/003/abstract.html.

[44] Martin Janssen, Marcus Metzler, and Martin R. Zirnbauer. Point-contact conductances at the quantum Hall transition. *Physical Review B*, 59(24):15836–15853, 6 1999. ISSN 0163-1829. doi: 10.1103/PhysRevB.59.15836. URL https://link.aps.org/doi/10.1103/PhysRevB.59.15836.

[45] A Katok. LYAPUNOV EXPONENTS, ENTROPY AND PERIODIC ORBITS FOR DIFFEOMORPHISMS. *of Rufus Bowen*, 1947. URL http://www.numdam.org/article/PMIHES_1980__51__137_0.pdf.

[46] V.A. KAZAKOV. Percolation on a Fractal with the Statistics of Planar Feynman Graphs: Exact Solution. *Modern Physics Letters A*, 04(17):1691–1704, 9 1989. ISSN 0217-7323. doi: 10.1142/S0217732389001921. URL http://www.worldscientific.com/doi/abs/10.1142/S0217732389001921.

[47] MG Kendall. *Advanced Theory Of Statistics Vol-I*. 1943. URL https://sci-hub.tw/http://krishikosh.egranth.ac.in/bitstream/1/2048308/1/0029_3095A.pdf.

[48] Sh. Khachatryan, A. Sedrakyan, and P. Sorba. Network models: Action formulation. *Nuclear Physics B*, 825(3):444–465, 2 2010. ISSN 0550-3213. doi: 10.1016/J.NUCLPHYSB.2009.09.033. URL https://www.sciencedirect.com/science/article/pii/S0550321309005161?via%3Dihub.

[49] Shahane Khachatryan, Robert Schrader, and Ara Sedrakyan. GrassmannGaussian integrals and generalized star products. *Journal of Physics A: Mathematical and Theoretical*, 42(30):304019, 7 2009. ISSN 1751-8113. doi: 10.1088/1751-8113/42/30/304019. URL http://stacks.iop.org/1751-8121/42/i=30/a=304019?key=crossref.261f02130be4615cf3b1960c708be1a4.

[50] V.G. Knizhnik, A.M. Polyakov, and A.B. Zamolodchikov. Fractal Structure of 2D-Quantum Gravity. *Modern Physics Letters A*, 03(08):819–826, 7 1988. ISSN 0217-7323. doi: 10.1142/S0217732388000982. URL http://www.worldscientific.com/doi/abs/10.1142/S0217732388000982.

[51] R. B. Laughlin. Quantized Hall conductivity in two dimensions. *Physical Review B*, 23(10):5632–5633, 5 1981. ISSN 0163-1829. doi: 10.1103/PhysRevB.23.5632. URL https://link.aps.org/doi/10.1103/PhysRevB.23.5632.

[52] M. J Lea, A. O Stone, and P Fozooni. The Hall Effect in 2D Electrons on Liquid Helium. *Europhysics Letters (EPL)*, 7(7):641–646, 12 1988. ISSN 0295-5075. doi: 10.1209/0295-5075/7/7/012. URL http://stacks.iop.org/0295-5075/7/i=7/a=012?key=crossref.d975e9ce1bd20aeda723fa6e8f10f2bf.

[53] Dung-Hai Lee. Network models of quantum percolation and their field-theory representations. *Physical Review B*, 50(15):10788–10791, 10 1994. ISSN 0163-1829. doi: 10.1103/PhysRevB.50.10788. URL https://link.aps.org/doi/10.1103/PhysRevB.50.10788.

[54] Dung-Hai Lee and Ziqiang Wang. Effects of Electron-Electron Interactions on the Integer Quantum Hall Transitions. *Physical Review Letters*, 76(21):4014–4017, 5 1996. ISSN 0031-9007. doi: 10.1103/PhysRevLett.76.4014. URL https://link.aps.org/doi/10.1103/PhysRevLett.76.4014.

[55] Wanli Li, C. L. Vicente, J. S. Xia, W. Pan, D. C. Tsui, L. N. Pfeiffer, and K. W. West. Scaling in Plateau-to-Plateau Transition: A Direct Connection of Quantum Hall Systems with the Anderson Localization Model. *Physical Review Letters*, 102 (21):216801, 5 2009. ISSN 0031-9007. doi: 10.1103/PhysRevLett.102.216801. URL https://link.aps.org/doi/10.1103/PhysRevLett.102.216801.

[56] Elliott H. Lieb. Solution of the Dimer Problem by the Transfer Matrix Method. In *Condensed Matter Physics and Exactly Soluble Models*, pages 537–539. Springer Berlin Heidelberg, Berlin, Heidelberg, 2004. doi: 10.1007/978-3-662-06390-3{_}34. URL http://link.springer.com/10.1007/978-3-662-06390-3_34.

[57] Andreas W. W. Ludwig, Matthew P. A. Fisher, R. Shankar, and G. Grinstein. Integer quantum Hall transition: An alternative approach and exact results. *Physical Review B*, 50(11):7526–7552, 9 1994. ISSN 0163-1829. doi: 10.1103/PhysRevB.50.7526. URL https://link.aps.org/doi/10.1103/PhysRevB.50.7526.

[58] Mikio Nakahara. Geometry and Topology in Physics. Technical report. URL https://cds.cern.ch/record/640926/files/0750306068_TOC.pdf.

[59] Gian Niu, D J Thouless, and Yong-Shi Wu. Quantized Hall conductance as a topological invariant. Technical Report 6, 1985. URL https://journals.aps.org/prb/pdf/10.1103/PhysRevB.31.3372.

[60] W. Nuding, A. Klümper, and A. Sedrakyan. Localization length index and subleading corrections in a Chalker-Coddington model: A numerical study. *Physical Review B*, 91(11):115107, 3 2015. ISSN 1098-0121. doi: 10.1103/PhysRevB.91.115107. URL https://link.aps.org/doi/10.1103/PhysRevB.91.115107.

[61] H. Obuse, A. R. Subramaniam, A. Furusaki, I. A. Gruzberg, and A. W. W. Ludwig. Boundary Multifractality at the Integer Quantum Hall Plateau Transition: Implications

for the Critical Theory. *Physical Review Letters*, 101(11):116802, 9 2008. ISSN 0031-9007. doi: 10.1103/PhysRevLett.101.116802. URL https://link.aps.org/doi/10.1103/PhysRevLett.101.116802.

[62] H. Obuse, A. R. Subramaniam, A. Furusaki, I. A. Gruzberg, and A. W. W. Ludwig. Conformal invariance, multifractality, and finite-size scaling at Anderson localization transitions in two dimensions. *Physical Review B*, 82(3):035309, 7 2010. ISSN 1098-0121. doi: 10.1103/PhysRevB.82.035309. URL https://link.aps.org/doi/10.1103/PhysRevB.82.035309.

[63] Hideaki Obuse, Ilya A. Gruzberg, and Ferdinand Evers. Finite-Size Effects and Irrelevant Corrections to Scaling Near the Integer Quantum Hall Transition. *Physical Review Letters*, 109(20):206804, 11 2012. ISSN 0031-9007. doi: 10.1103/PhysRevLett.109.206804. URL https://link.aps.org/doi/10.1103/PhysRevLett.109.206804.

[64] RB Paris and D Kaminski. *Asymptotics and mellin-barnes integrals*. 2001. URL https://sci-hub.tw/https://books.google.com/books?hl=en&lr=&id=LtOfHnClUSEC&oi=fnd&pg=PA1&dq=mellin+barnes&ots=s5cYON9L9m&sig=7B3dcyojAXUKTDYJY6gWVd378J0.

[65] Andrea Pelissetto and Ettore Vicari. Critical phenomena and renormalization-group theory. *Physics Reports*, 368(6):549–727, 10 2002. ISSN 03701573. doi: 10.1016/S0370-1573(02)00219-3. URL http://linkinghub.elsevier.com/retrieve/pii/S0370157302002193.

[66] A.M. Polyakov. Quantum geometry of bosonic strings. *Physics Letters B*, 103(3):207–210, 7 1981. ISSN 0370-2693. doi: 10.1016/0370-2693(81)90743-7. URL https://www.sciencedirect.com/science/article/pii/0370269381907437.

[67] D. G. Polyakov and B. I. Shklovskii. Conductivity-peak broadening in the quantum Hall regime. *Physical Review B*, 48(15):11167–11175, 10 1993. ISSN 0163-1829. doi: 10.1103/PhysRevB.48.11167. URL https://link.aps.org/doi/10.1103/PhysRevB.48.11167.

[68] D. G. Polyakov and B. I. Shklovskii. Variable range hopping as the mechanism of the conductivity peak broadening in the quantum Hall regime. *Physical Review Letters*, 70(24):3796–3799, 6 1993. ISSN 0031-9007. doi: 10.1103/PhysRevLett.70.3796. URL https://link.aps.org/doi/10.1103/PhysRevLett.70.3796.

[69] D. G. Polyakov and B. I. Shklovskii. Variable range hopping as the mechanism of the conductivity peak broadening in the quantum Hall regime. *Physical Review Letters*, 70(24):3796–3799, 6 1993. ISSN 0031-9007. doi: 10.1103/PhysRevLett.70.3796. URL https://link.aps.org/doi/10.1103/PhysRevLett.70.3796.

[70] A. M. M Pruisken and M. A Baranov. Cracking Coulomb Interactions in the Quantum Hall Regime. *Europhysics Letters (EPL)*, 31(9):543–548, 9 1995. ISSN 0295-5075. doi: 10.1209/0295-5075/31/9/007. URL http://stacks.iop.org/0295-5075/31/i=9/a=007?key=crossref.ea35ba7040e3da05bfc25c2fc629a96c.

[71] A. M. M. Pruisken and I. S. Burmistrov. Non-fermi liquid criticality and superuniversality in the quantum hall regime. *JETP Letters*, 87(4):220–224, 4 2008. ISSN 0021-3640. doi: 10.1134/S0021364008040097. URL http://link.springer.com/10.1134/S0021364008040097.

[72] A.M.M. Pruisken. On localization in the theory of the quantized hall effect: A two-dimensional realization of the θ-vacuum. *Nuclear Physics B*, 235(2):277–298, 6 1984. ISSN 05503213. doi: 10.1016/0550-3213(84)90101-9. URL http://linkinghub.elsevier.com/retrieve/pii/0550321384901019.

[73] Martin Puschmann, Philipp Cain, Michael Schreiber, and Thomas Vojta. Integer quantum Hall transition on a tight-binding lattice. 2018. URL https://arxiv.org/pdf/1805.09958.pdf.

[74] P J Reynolds, H E Stanley, and W Klein. A real-space renormalization group for site and bond percolation. *Journal of Physics C: Solid State Physics*, 10(8):L167–L172, 4 1977. ISSN 0022-3719. doi: 10.1088/0022-3719/10/8/002. URL http://stacks.iop.org/0022-3719/10/i=8/a=002?key=crossref.c95f3a7539c5ac58a022cf521c8e5ff2.

[75] Abraham. Savitzky and M. J. E. Golay. Smoothing and Differentiation of Data by Simplified Least Squares Procedures. *Analytical Chemistry*, 36(8):1627–1639, 7 1964. ISSN 0003-2700. doi: 10.1021/ac60214a047. URL http://pubs.acs.org/doi/abs/10.1021/ac60214a047.

[76] Ara Sedrakyan. Action formulation of the network model of plateau-plateau transitions in the quantum Hall effect. *Physical Review B*, 68(23):235329, 12 2003. ISSN 0163-1829. doi: 10.1103/PhysRevB.68.235329. URL https://link.aps.org/doi/10.1103/PhysRevB.68.235329.

[77] T. Senthil and Matthew P. A. Fisher. Quasiparticle localization in superconductors with spin-orbit scattering. *Physical Review B*, 61(14):9690–9698, 4 2000. ISSN 0163-1829. doi: 10.1103/PhysRevB.61.9690. URL https://link.aps.org/doi/10.1103/PhysRevB.61.9690.

[78] Keith Slevin and Tomi Ohtsuki. Critical exponent for the quantum Hall transition. 2009. URL https://arxiv.org/pdf/0905.1163.pdf.

[79] Keith Slevin and Tomi Ohtsuki. Finite Size Scaling of the Chalker-Coddington Model. 3 2012. doi: 10.1142/s2010194512006162. URL https://arxiv.org/abs/1203.1384.

[80] Dietrich. Stauffer and Amnon. Aharony. *Introduction to percolation theory*. Taylor & Francis, second edition, 1994. ISBN 0748402535.

[81] Masuo Suzuki. Transfer-matrix method arid Monte Carlo simulation in quantum spin systems. URL https://0-journals-aps-org.pugwash.lib.warwick.ac.uk/prb/pdf/10.1103/PhysRevB.31.2957.

[82] David Tong. Lectures on the Quantum Hall Effect. 6 2016. URL https://arxiv.org/abs/1606.06687.

[83] Daniel C. Tsui. Nobel Lecture: Interplay of disorder and interaction in two-dimensional electron gas in intense magnetic fields. *Reviews of Modern Physics*, 71(4):891–895, 7 1999. ISSN 0034-6861. doi: 10.1103/RevModPhys.71.891. URL https://link.aps.org/doi/10.1103/RevModPhys.71.891.

[84] Klaus von Klitzing. The quantized Hall effect. *Reviews of Modern Physics*, 58(3):519–531, 7 1986. ISSN 0034-6861. doi: 10.1103/RevModPhys.58.519. URL https://link.aps.org/doi/10.1103/RevModPhys.58.519.

[85] Ziqiang Wang, Matthew P. A. Fisher, S. M. Girvin, and J. T. Chalker. Short-range interactions and scaling near integer quantum Hall transitions. *Physical Review B*, 61(12):8326–8333, 3 2000. ISSN 0163-1829. doi: 10.1103/PhysRevB.61.8326. URL https://link.aps.org/doi/10.1103/PhysRevB.61.8326.

[86] Wigner and E.P. Measurement of quantum-mechanical operations; Die Messun Quantenmechanischer Operatoren, 7 1952. URL https://www.osti.gov/biblio/4866969.

[87] Kenneth G. Wilson. The renormalization group and critical phenomena. *Reviews of Modern Physics*, 55(3):583–600, 7 1983. ISSN 0034-6861. doi: 10.1103/RevModPhys.55.583. URL https://link.aps.org/doi/10.1103/RevModPhys.55.583.

[88] F. Y. Wu. The Potts model. *Reviews of Modern Physics*, 54(1):235–268, 1 1982. ISSN 0034-6861. doi: 10.1103/RevModPhys.54.235. URL https://link.aps.org/doi/10.1103/RevModPhys.54.235.

[89] Martin R Zirnbauer. Conformal Field Theory of the Integer Quantum Hall Plateau Transition. 1999. URL https://arxiv.org/pdf/hep-th/9905054.pdf.